

## **Response to Reviewer # 1**

Authors would like to thank the anonymous reviewer for thorough evaluation of our manuscript and constructive comments. Point-by-point responses to the reviewer's comments are given below in bold fonts and corresponding changes in the manuscript have been highlighted in red color.

**General comment:** This article delineates the effects of spatial resolution on the model performance over the central Himalaya. Ground and radiosonde profiles were used to assess the performance of WRF at different spatial resolution. The temporal evolution of meteorological profiles in WRF is seen to be in agreement with the measurements with stronger correlations for upper troposphere than those in the lower troposphere. To use the profiles to assess the model result for mountain region is new in my review. However, I find that this paper does not really reach to main question for mountain meteorology studies. The authors should review the frontier of this area. Only do evaluations is not qualified for GMDD publication.

**Response:** We agree with the reviewer and following the suggestion more literature survey has been included in the revised version (Page: 4-5, Lines: 85-104). We would like to mention that our study is not limited to evaluation only and we show that high-resolution set ups, with existing terrains in the model preprocessor, could reduce the model biases only to some extent. We therefore implemented a very high-resolution topography into the preprocessor to improve the model performance. Some biases particularly in the dynamics suggests uncertainties associated with other factors e.g. interaction between local circulation due to slope winds and synoptic-scale flow, or the representation of highly complex topography of the Himalaya, as correctly pointed out by the reviewer. This study is therefore first step and would be followed up with testing of individual physics schemes as new field measurements

**become available. These aspects and outlook have been discussed in the revised version (Page: 20-21 Lines 373-406; Page: 25-27 Lines: 503-505, 509-514). It must be however stressed that a model evaluation does qualify for GMD(D) publications as mentioned in the journal's policy.**

**Comment 1:** An issue is that when they compare model grid values with that of AWS, they might use two temperature at different height. Please compare the AWS elevation and the grid elevation where AWS located. Use the elevation difference to adjust the model temperature. The same problem also happens to wind speed. There are many evaluation papers for the mountain numerical simulation. The authors should review these papers, try to improve the wind speed performance.

**Response 1: Thanks for the valuable suggestion. The difference between actual elevation of the observation site with model grid is 588 m in d01, 480 m in d02, and 270 m in d03 respectively. As the objective here is to describe the improvements in the model output over finer resolutions, we have analyzed model output without adjustments first. Nevertheless, following reviewer's suggestion and following other mountain modelling papers (e.g. Mues et al., 2018), meteorological data adjusted for elevation has also been analyzed in the revised manuscript (Page: 20, Lines: 371-390 and revised Table 1).**

**Comment 2:** Figure 3, add their difference between d01 and Radiosonde and give some introduction on the difference. Line 261, it's better to add a figure which shows the correlation coefficient  $r$ , mean bias etc. result for all the height, not only say model captures variations at 500 hPa better than 50 hPa. It is also possible to compare the  $r$  and mean bias profiles with the three spatial resolution simulation.

**Response 2:** As suggested, difference between d01 and radiosonde are analyzed and discussed (revised Figure 3; and Page: 13-14, Lines: 269-282). Correlations at different altitudes are presented in form of Taylors diagram (Figure 7a). Following reviewer's suggestion, results summarizing the mean bias, root mean square error, correlation of profiles at different resolution have also been included in the revised version (new Figure 5, and Page: 15-16, Lines: 307-331).

**Comment 3:** Figure 4, many things are not clear in the figure, which year? It also repeat with figure 3. Again, the difference is more interesting to us.

**Response 3:** Following reviewer's suggestions, Figure 4 (as well as Figure 3) have been modified for clarity. Year (2011) has been mentioned on the revised figure. As suggested, differences are presented in both the figures in revised version.

**Comment 4:** Figure 6 the figure legend is not clear at all. Replot the figure with a colored marker.

**Response 4:** As suggested, Figure 6 (Figure 7 in the revised version) has been replotted with proper color marker and legend.

**Comment 5:** Figure 7 where is (a) and (b) letters? what does "0-6-12-.30" mean in the first wind-rose diagram? then why 0-2, 2-4, 4-6.....legend appears on the right of the fourth diagram?

**Response 5:** Figure 7 (Figure 8 in the revised version) has been revised to address reviewer's comment. Frequency of the occurrence and detailed legends are included now. Previously,

the “0-6-12-..30” was percentage frequency and legend “0-2, 2-4, 4-6.....” at the right of the figure was showing the wind speed ( $\text{ms}^{-1}$ ).

**Comment 6:** Figure 8, the simulation does not show the diurnal variation in wind speed at all. What’s the explanation for it? This is really interesting for mountain numerical simulation.

**Response 6:** We agree that the model does not capture the diurnal variation in the wind speed, as also seen over another complex terrain – such as the Tibetan Plateau (Zhou et al., 2019). The daytime reduction in the wind speed was observed by Solanki et al. (2019) over the same mountain peak attributed to the evolution of mountain circulation due to the heating of the slopes and its interaction with the synoptic scale flow, resulting in increased intensity of turbulences and vertical exchange of the momentum fluxes within the surface layer of atmosphere which inhibit the synoptic scale flow up to a certain extent during the daytime. Such competing effect between the thermal and mechanical driven processes could remain unresolved in the model even at higher grid resolution. In addition, mountain winds show sensitivity to boundary layer schemes Yver et al. (2013). Here, we analysed first the impacts of improved representation of the topographical features which would be followed up with testing of different physics schemes in the future. The interpretations with references as well as the limitations and outlook is added in the revised version of the manuscript (Page: 20-21; Lines: 371-406).

## **Reply to comments of Reviewer#2**

Authors would like to thank the anonymous reviewer for thorough evaluation of our manuscript and constructive comments. Point-by-point responses to the reviewer's comments are given below in bold fonts and corresponding changes in the manuscript have been highlighted in red color.

**General comment:** This study uses WRF v3.8.1 to explore the effects of spatial resolution on local meteorology. It is very interesting that they found the finer spatial resolution can reduce the biases in simulated meteorology and improve representation of CH through domain feedback into regional-scale simulations. However, in this study, there are too many descriptions of the simulation, but no enough physical explanation to the simulation. It's difficult to make sense that why it occurred. In my view, this manuscript still needs major revision before it can be accepted.

**Response:** Thanks for the suggestion. Here, we mainly show that more realistic representation of the highly complex terrain, through finer resolution implemented with 3s terrain data leads to better local meteorology of the central Himalaya. Following reviewer's suggestion more discussions including physical explanations have been presented in the revised version of the manuscript, as described in response to specific comments.

**Comment 1:** Section 2.2: How do you process the different temporal resolution of datasets, using the mean value or instantaneous value?

**Response 1:** Collocated instantaneous values between model and observations have been compared. This is mentioned in the revised manuscript (Page: 9; Lines: 188-189).

**Comment 2:** Line 182-184: It is available of ERA interim at  $0.125^{\circ} \times 0.125^{\circ}$ , but it's the interpolation results, which may not represent the true performance of ERA interim, especially over the complex terrain regions. It's better to add the comparison between WRF and ERA interim at  $0.75^{\circ} \times 0.75^{\circ}$ , even there is much less grids of ERA in D03.

**Response 2:** As suggested, ERA interim at  $0.75 \times 0.75^{\circ}$  has been used for comparison in the revised manuscript (Figure 2; Pages:10-12; Lines: 204; 245-246).

**Comment 3:** Please update the figure captions: i.e., units of all the variables in Figure 3; caption of Figure 6 is not clear (Fig 6a is the comparison between WRF simulation at D01 and the observation?); Figure 8 is only focused D01, etc. you should make them clear in figure caption.

**Response 3:** Thanks for pointing this out. We have revised the figure and provided clear caption with details of units. Radiosonde and model d01 is also marked clearly (please see Figures 3, 7a, and 9 in the revised version).

**Comment 4:** Line 259-262: Why did it happen? The different vertical distribution and the lower correlation at lower altitudes mostly come from the influence of land-air interaction. Please discussing the possible factors of your results.

**Response 4:** We agree that the interactions of the underlying surface with lower troposphere profoundly affects the dynamics and local circulations. In mountainous terrains, most important interactions include slope winds and the synoptic scale flow (Solanki et al., 2019). Orographic drag has been suggested to be additional source of the lower correlation (Zhou

et al., 2018, 2019). This is discussed in the revised version of the manuscript (Page: 16 Lines: 312-322; Page: 20-21 Lines: 382-406).

**Comment 5:** How do you process the different spatial representation of different simulation and observation? For D01, one grid can indicate the mean situation of 15\*15km area; meanwhile, for D02, it only indicates that in 5\*5km area, etc. please show details of your methods to compare the grid simulation and the in-situ observation.

**Response 5:** The nearest grid point to the observational site is used for comparison (Page: 9; Lines: 188-189) (e.g. Mues et al., 2018; Singh et al., 2016).

**Comment 6:** Line 286-287: It's very interesting that WRF shows a warm bias south side of Himalaya. Many previous studies pointed that there is obvious cold bias over Tibet (including Himalaya), i.e., Zhou et al. (2017) and Gao et al. (2015). Did you check your location of observation site and WRF grids? The warm bias in your WRF simulation is due to the lower terrain height of the grids than the Observed, please check if they are located over valley and the observed located over ridge

**Response 6:** Thanks for valuable suggestion. The observation site is a mountain ridge. We performed further analysis of model output by accounting for the altitude difference through linear interpolation of the meteorological parameters to the actual altitude of site in the revised version (Figure 6d-f, Table 1). Altitude adjusted data of model shows cold bias in

**agreement with Gao et al., (2015). This is discussed in the revised version of the manuscript (Page: 20-21; Lines: 371-399).**

**Comment 7:** Figure 5: as the WRF resolution increasing, the diurnal cycle simulation of T and RH are better, but it didn't work for wind speed. please check the location of the WRF grids and observed station, if both them located valley or ridge? Besides, Zhou et al. (2019) stressed the importance of turbulent orographic form drag (TOFD) on the diurnal cycle simulation of wind speed. It's better to give more explains of inconsistent diurnal cycle of wind between simulation and observations.

**Response 7: The processes such as local circulation, slope wind interaction with the synoptic-scale flow are the key factors governing the diurnal winds over mountain ridge, as shown in Solanki et al., (2016, 2019). We agree with reviewer's view that turbulent orographic form drag (TOFD) could modify the diurnal evolution of wind over such terrains (Zhou et al (2019). These all aspects with relevant references have been included in the revised version of the manuscript (Page: 20-21; Lines:382-406).**

**Comment 8:** RH is also dependent on Temperature. What's the performance of the WRF in simulation Specific Humidity (Q)? Please compare the Q between WRF simulation and observation.

**Response 8: Comparison of specific humidity between model and observations has been investigated (new Figure S1 in the Supplement). The specific humidity (Q2) shows the**

**explicit dependent on the horizontal grid resolution the bias decreases with increasing the grid resolution. The Q2 shows better correlation (0.67 for d01, 0.72 for d02, and 0.77 for d03) than RH (0.43 for d01, 0.45 for d02 and 0.52 for d03). This is discussed in the revised version of the manuscript (Page: 18; Lines: 350-354).**

**Comment 9:** Section 3.4: What are the effects of feedback on the wind direction? In WRF-WF experiments, there are obvious difference among the simulated wind direction at three resolutions. Is there any improvement in the WRF-F experiments?

**Response 9:** The slight improvement in the wind direction is observed in WRF-F, such improvements are explained in the corresponding section 3.4 (Page 24, Line 459-462), where the effect of the feedback is discussed and changes can be seen in the wind rose plot as shown in Figure S2 and S3. Nevertheless, smaller changes were seen in correlations for WS10 (by 0.05) and T2 (by -0.02) (Figure S2). Variations in wind speed and direction shows an improvement in dominant flow direction e.g. easterly, westerly and north-westerly (Figure S3).

**Comment 10:** Section 3.5: You should check the orographic variation in WRF model output, when you input different geographic data. multi-scale orographic variations are key factors of Wind and moisture simulation over complex terrain, i.e., south side of Himalaya (Wang et al., 2020).

**Response 10:** The orographic variations in WRF model output have been checked for different geographical input data (Figure 11, Figure S6). As suggested, the spatial

**distribution of relative humidity is included in the revised version of the manuscript (new Figure S6; Page:27-28; Lines:525-529). The impact of the orographic variation with different resolution topographic data in RH (Figure S6) shows the differences are in range of -1 to 1% in d02 and -3% to 3% in d03. Such variations are due to inclusion of the SRTM3s high resolution topographic data allowing the model to capture more variation, such orographic features are seen to impact the distribution of moisture in line with suggested study (Wang et al., 2020).**

1 **Effects of spatial resolution on WRF v3.8.1 simulated meteorology over the central**  
2 **Himalaya**

3 **Jaydeep Singh<sup>1</sup>, Narendra Singh<sup>1\*</sup>, Narendra Ojha<sup>2</sup>, Amit Sharma<sup>3,a</sup>, Andrea Pozzer<sup>4,5</sup>, Nadimpally**  
4 **Kiran Kumar<sup>6</sup>, Kunjukrishnapillai Rajeev<sup>6</sup>, Sachin S. Gunthe<sup>3</sup>, V. Rao Kotamarthi<sup>7</sup>**

5 <sup>1</sup>Aryabhata Research Institute of Observational Sciences, Nainital, India

6 <sup>2</sup>Physical Research Laboratory, Ahmedabad, India

7 <sup>3</sup>EWRE Division, Department of Civil Engineering, Indian Institute of Technology Madras, Chennai,  
8 India

9 <sup>4</sup>Department of Atmospheric Chemistry, Max Planck Institute for Chemistry, Mainz, Germany

10 <sup>5</sup>Earth System Physics Section, International Centre for Theoretical Physics, Trieste, Italy

11 <sup>6</sup>Space Physics Laboratory, Vikram Sarabhai Space Centre, Thiruvananthapuram, India

12 <sup>7</sup>Environmental Science Division, Argonne National Laboratory, Argonne, Illinois, USA

13 <sup>a</sup>Now at Department of Civil and Infrastructural Engineering, Indian Institute of Technology Jodhpur,  
14 Jodhpur, India

15 **Correspondence:** Narendra Singh (narendra@aries.res.in) and Andrea Pozzer (andrea.pozzer@mpic.de)

16

17 **Abstract**

18 The sensitive and fragile ecosystem of the central Himalayan (CH) region, experiencing enhanced  
19 anthropogenic pressure, requires adequate atmospheric observations and an improved representation of  
20 Himalaya in the models. However, the accuracies of atmospheric models remain limited here due to highly  
21 complex mountainous topography. This article delineates the effects of spatial resolution on the modeled  
22 meteorology and dynamics over the CH by combining the WRF (Weather Research and Forecasting)  
23 model with the GVAX (Ganges Valley Aerosol Experiment) observations during the summer monsoon.  
24 WRF simulation is performed over a domain (d01) encompassing northern India at 15 km x 15 km

25 resolution, and two nests: d02 (5 km x 5 km) and d03 (1 km x 1 km) centered over CH with boundary  
26 conditions from respective parent domains. WRF simulations reveal higher variability in meteorology e.g.  
27 Relative Humidity (RH=70.3–96.1%), Wind speed (WS=1.1–4.2 ms<sup>-1</sup>), as compared to the ERA Interim  
28 reanalysis (RH=80.0–85.0, and WS=1.2–2.3ms<sup>-1</sup>) over the northern India owing to higher resolution. WRF  
29 simulated temporal evolution of meteorological profiles is seen to be in agreement with the balloon-borne  
30 measurements with stronger correlations aloft (r = 0.44–0.92), than those in the lower troposphere (r =  
31 0.18–0.48). However, the model overestimates temperature (warm bias by 2.8°C) and underestimates RH  
32 (dry bias by 6.4%) at surface in the d01. Model results show a significant improvement in d03 (P=827.6  
33 hPa, T=19.8°C, RH=92.3%) and are closer to the GVAX observations (P=801.4, T=19.5, RH=94.7%).  
34 **Interpolating coarser simulation (d01, d02) to the altitude of station reduces the biases in pressure and**  
35 **temperature, however, suppresses the diurnal variations highlighting significance of well-resolved terrain**  
36 **effects (d03).** Temporal variations in near-surface P, T and RH are also reproduced by WRF d03 to an  
37 extent (r > 0.5). A sensitivity simulation incorporating the feedback from nested domain demonstrated  
38 improvements in simulated P, T and RH over CH. Our study shows the WRF model set up at finer spatial  
39 resolution can significantly reduce the biases in simulated meteorology and such an improved  
40 representation of CH can be adopted through domain feedback into regional-scale simulations.  
41 Interestingly, WRF simulates a dominant easterly wind component at 1 km x 1 km resolution (d03), which  
42 was missing in the coarse simulations; however, a frequent southeastward wind component remained  
43 underestimated. Model simulation implementing a high resolution (3 s) topography input (SRTM)  
44 improved the prediction of wind directions, nevertheless, further improvements are required to better  
45 reproduce the observed local-scale dynamics over the CH.

## 46 **1. Introduction**

47 Himalayan region is one of the most complex and fragile geographical systems in the world, and has  
48 paramount importance for the climatic implications and air composition at regional to global scales (e.g.

49 Lawrence et al., 2010, Pant et al., 2018; Lelieveld et al., 2018). The ground-based observations of  
50 meteorology and fine-scale dynamics are highly sparse. In this direction, an intensive field campaign  
51 called as the GVAX (Kotamarthi, 2013) was carried out over a mountainous site in the Central Himalaya  
52 which provided valuable meteorological observations for atmospheric research, model evaluation and  
53 improvements. Accurate simulations of meteorology are needed for numerous investigations, such as to  
54 study the regional and global climate change, snow-cover change, trapping and transport of regional  
55 pollution, and the hydrological cycle especially monsoon system (e. g. Sharma and Ganju, 2000; Bhutiyani  
56 et al., 2007; Pant et al., 2018). Studies focussing over this region have become more important due to the  
57 increasing anthropogenic influences resulting in enhanced levels of Short-Lived Climate forcing Pollutants  
58 (SLCPs) along the Himalayan foothills (e. g. Ojha et al., 2012; Sarangi et al., 2014; Rupakheti et al., 2017;  
59 Deep et al., 2019; Ojha et al., 2019). Although Global Climate Models (GCMs) simulate the climate  
60 variabilities over global scale, their application for reproducing observations in the regions of complex  
61 landscapes is limited, due to coarse horizontal resolution (e. g. Wilby et al., 1999; Boyle et al. 2010;  
62 Tselioudis et al., 2012; Pervez and Henebry, 2014; Meher et al., 2017). Mountain ridges, rapidly changing  
63 land-cover, and the low altitude valleys often lie within a grid box of typical global climate models  
64 resulting in significant biases in model results when compared with observations (e. g. Ojha et al., 2012;  
65 Tiwari et al., 2017, Pant et al., 2018). On the other hand, Regional Climate Models (RCMs) at finer  
66 resolutions allow better representation of the topographical features thus providing improved simulations  
67 of the atmospheric variability over regions of complex terrains. Several mesoscale models (e. g.  
68 Christensen et al., 1996; Caya and Laprise 1999; Skamarock et al., 2008; Zadra et al., 2008) have been  
69 developed and applied successfully over different parts of the world. These studies have revealed that the  
70 RCMs provide significant new insights by parameterizing or explicitly simulating atmospheric processes  
71 over finer spatial scales. Nevertheless, large uncertainties are still seen over highly complex areas  
72 indicating the effects of further unresolved terrain features (e. g. Wang et al., 2004; Laprise, 2008; Foley,  
73 2010) and need to improve the simulations.

74 Of late, anthropogenic influences and climate forcing have been increasing over the Himalaya and its  
75 foothill regions since pre-industrial times (Pant et al., 2006; Bonasoni et al., 2012; Srivastava et al., 2012).  
76 Further, an increase in the intensity and frequency of extreme weather events have been observed over the  
77 Himalayan region (e. g. Nandargi and Dhar, 2012; Sun et al., 2017; Dimri et al., 2017) in past few decades.  
78 These events include extreme rainfall and resulting flash floods, cloudbursts, landslides etc., and their  
79 causes range from mesoscale processes to larger synoptic scale events. Unfortunately, the lack of  
80 observational network covering the Himalaya and foothills with sufficient spatio-temporal density inhibits  
81 the detailed understanding of the aforementioned processes, and meteorological and dynamical conditions  
82 in the region. Therefore, usage of regional models, evaluated against available in-situ measurements would  
83 fill the gap of investigating atmospheric variability in the observationally sparse and geographically  
84 complex mountain terrain of Himalaya.

85 The biases in simulating the meteorological parameters especially in the lower troposphere are associated  
86 with several factors e.g. representation of topography, land use, surface heat and moisture flux transport,  
87 and parameterization of physical processes (e. g. Lee et al., 1989; Hann and Yang, 2001; Cheng and  
88 Steenburgh, 2005; Singh et al., 2016). WRF model has been applied over the complex terrains in the  
89 Himalaya region (e.g. Sarangi et al., 2014; Singh et al., 2016, Mues et al., 2018; Wang et al., 2020), Tibetan  
90 Plateau (e.g. Gao et al., 2015; Zhou et al., 2018), and intermountain west of the United States (e.g. Zhang  
91 et al., 2013) to evaluate and study the meteorology and dynamics. A cold bias was reported in this model  
92 over the Tibetan Plateau and Himalayan region by Gao et al (2015). Near surface winds showed biases  
93 linked with unresolved processes in the model such as sub-grid turbulence, land-surface atmospheric  
94 interactions, besides boundary layer parametrization (Hanna and Yang, 2001; Zhang and Zheng, 2004;  
95 Cheng and Steenburgh, 2005). Zhou et al., (2018) found lower biases in simulated winds after taking into  
96 account the turbulent orographic form drag over the Tibetan Plateau.

97 WRF model with suitably chosen schemes has been shown to reproduce the regional-scale meteorology  
98 (Kumar et al., 2012) and to some extent also the mountain-valley wind systems (Sarangi et al., 2014) and

99 boundary layer dynamics (Singh et al., 2016; Mues et al., 2018) over the Himalayan region. Nevertheless  
100 local meteorology is still difficult to simulate correctly; Mues et al (2018) performed high resolution WRF  
101 simulation over Kathmandu valley of Himalaya and reported overestimation of 2m temperature and 10m  
102 wind speed attributed to complex topography even at resolution of 3 km x 3 km. Meteorological  
103 simulations including winds and precipitation were shown to improve with increase in grid resolution over  
104 different parts of the world (e.g. Mass et al., 2002; Rife and Davis, 2005; Hart et al., 2005).

105 Most of the studies carried out over the Himalayan region applied model at coarse horizontal resolutions  
106 (45 to 30 km) and evaluated simulations over larger spatial scales, except the study by Mues et al. (2018)  
107 which used relatively higher spatial resolution (3 km x 3 km). Nevertheless, it remains unclear how the  
108 finer resolution could better resolve the complex terrain of the central Himalaya and improve the  
109 meteorological simulations, especially at 5 km to 1 km resolution.

110 With this opportunity of model evaluation and improvements in simulating meteorological and dynamical  
111 variability over the CH, here, we have used a nested WRF set up with a coarse 15 km x 15 km domain  
112 (d01) with nests of 5 km x 5 km (d02) and 1 km x 1 km (d03) centred over the CH. The main objectives  
113 of the study are as follows:

- 114 1. To examine the model performance over the CH at 15 km x 15 km resolution
- 115 2. To examine the effects or improvements that can be achieved at higher spatial resolutions: 5 km x  
116 5 km, and 1 km x 1 km.
- 117 3. To investigate the effect of feedback from nest that could be adopted into parent domain, as this  
118 would allow configuring a setup covering larger Indian region with more accurate results over  
119 Himalaya
- 120 4. To implement a very high resolution (3 s) topographical input into the model to examine the  
121 potential of simulations finer than 1 km in reproducing local-scale dynamics

122 Subsequent section 2 describes the model set up, followed by experimental design, and a discussion of  
123 datasets used for model evaluation. Section 3 provides comparison of model results with the ERA Interim  
124 reanalysis (section 3.1), radiosonde observations (section 3.2), and ground-based measurements (section  
125 3.3). Analysis of domain feedback is presented in section 3.4, and the effect of implementing high-  
126 resolution topography is investigated in section 3.5, followed by the summary and conclusions in section  
127 4.

## 128 **2. Methodology**

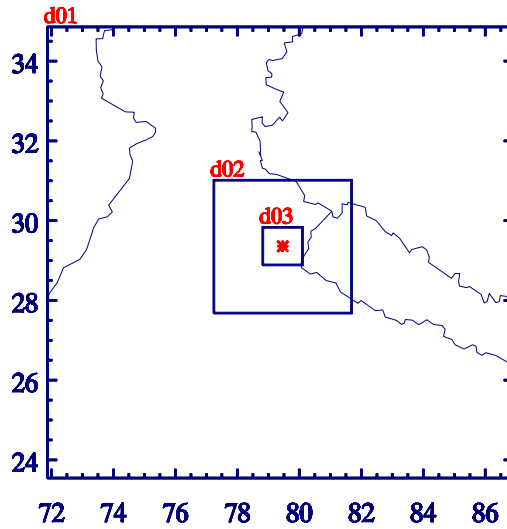
### 129 **2.1 Model set up and Experimental Design**

130 Weather Research and Forecasting (WRF) model—version 3.8.1 has been used in the present study. WRF  
131 is a mesoscale non-hydrostatic, Numerical Weather prediction (NWP) model with advance physics and  
132 numerical schemes for simulating meteorology and dynamics. WRF-ARW uses Eulerian mass based  
133 dynamical core with terrain-following vertical coordinates (Skamarock et al., 2008). ERA Interim  
134 reanalysis from the European Center for Medium Range Weather Forecasts (ECMWF) available at a  
135 horizontal resolution of  $0.75^0 \times 0.75^0$  at 6 h interval has been used to provide the initial and lateral boundary  
136 conditions to the WRF model (Dee et al., 2011). Static geographical data, which includes the information  
137 of terrain height, land use, and land cover etc., is based on the Moderate Resolution Imaging  
138 Spectroradiometer (MODIS) data available at 30s horizontal resolution.

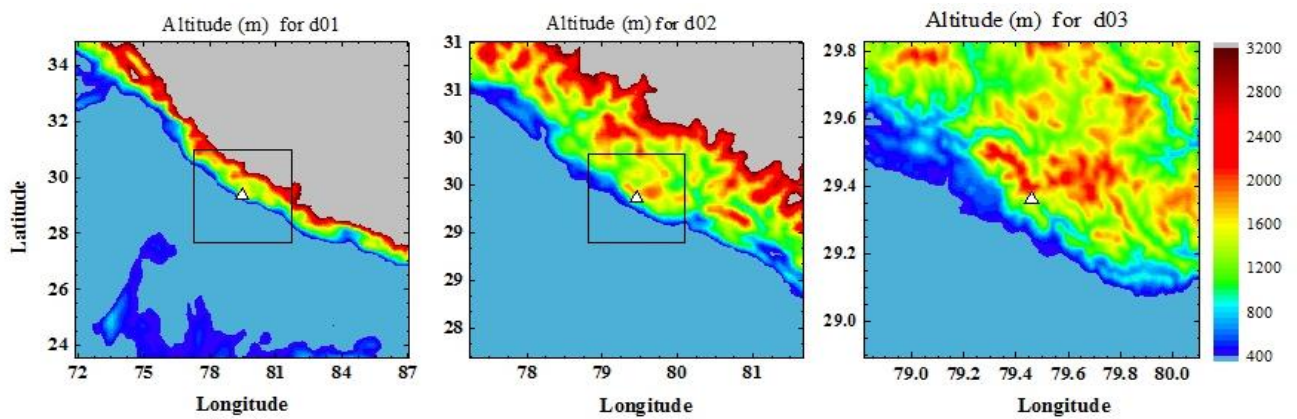
139 The shortwave radiation scheme used is the Goddard scheme (Chou and Suarez, 1994) while the long  
140 wave radiation is simulated by the Rapid Radiative Transfer Model (Mlawer et al., 1997) scheme. For  
141 resolving the boundary layer processes the first order nonlocal closure based Yonsei University (YSU)  
142 scheme (Hong et al., 2006) is used including an explicit entrainment layer with the K-profile in an unstable  
143 mixed layer. PBL height is determined from the Richardson number ( $Ri_b$ ) method in this PBL scheme.  
144 Convection is parameterized by the Kain-Fritsch (KF) cumulus parameterization (CP) scheme, accounting  
145 for sub-grid level processes in the model such as precipitation, latent heat release and vertical redistribution

146 of heat and moisture as a result of convection (Kain, 2004). With increase in model grid resolution to less  
147 than 10 km (known as “grey area”), the CP scheme is usually turned off and an explicit microphysics (MP)  
148 scheme is needed to resolve cloud and precipitation processes (Weisman et al., 1997). In the present study,  
149 the CP scheme is used for d01 while it is turned off for d02 and d03. The Thomson microphysics containing  
150 prognostic equations for cloud water, rain water, ice, snow, and graupel mixing ratios, is used (Thompson  
151 et al., 2004). Parameterization of surface processes is done with MM5 Monin-Obukhov scheme and  
152 Unified Noah land surface model (LSM) (Chen and Dudhia, 2001; Ek et al., 2003; Tewari et al., 2004).  
153 The Noah LSM includes a single canopy layer and four soil layers at 0.1, 0.2, 0.6 and 1m within 2m of  
154 depth (Ek et al., 2003).

155 The model is configured with three domains of 15 km (d01), 5 km (d02) and 1 km (d03) horizontal grid  
156 spacing using Mercator projection centering at Manora Peak (79.46°N, 29.36°E, amsl ~ 1936m) in central  
157 Himalaya. Topography within the model domains is highly complex as evident from the ridges (Figure 1).  
158 Outer domain d01 includes north part of Thar Desert, part of IGP (Indo-Gangetic-Plain), Himalayan  
159 mountains with vegetation and snow cover, while the innermost domain d03 consists of mostly  
160 mountainous terrain. Model atmosphere has 51 vertical levels with top at 10 hPa. For d01, 100 east-west  
161 and 86 north south grid points are used to account for the effect of synoptic scale meteorology e.g. Indian  
162 summer monsoon. The d02 has 88 east-west and 76 north-south grid points covering sufficient spatial  
163 region around the observational site to consider the effects of mesoscale dynamics, e.g. change of wind  
164 pattern due to orography. The innermost domain 03 has 126 east-west and 106 north-south grid points  
165 mainly to reveal local effects e.g. convection, advection, turbulence, orthographic lifting etc.



166



167

168 **Figure 1:** Topography in WRF model domains at three horizontal resolutions: domain d01 (15 x 15km),  
 169 domain d02 (5 x 5km) and domain d03 (1 x 1 km). Triangle symbol indicates the location of the GVAX  
 170 campaign over Manora Peak, Nainital. Box inside the figure represents the nested domain.

171 The d01 simulation provides the boundary conditions to domain d02, and domain d02 to innermost domain  
 172 d03. For d01, boundary conditions are provided from ERA Interim reanalysis, as explained earlier. Model  
 173 simulation has been performed for four months of the summer monsoon season: 01 June 2011 to 30  
 174 September 2011 (JJAS). First 10 days of the simulation is considered as the spin-up and removed from the  
 175 analysis. Only the outer domain d01 is nudged with the global reanalysis for temperature, water vapor,  
 176 zonal and meridional (u and v) components of wind with nudging coefficient of 0.0006 ( $6 \times 10^{-4}$ ) at all  
 177 vertical levels (e.g. Kumar et al., 2012). Several of the configuration options e. g. physics, meteorological

178 nudging, etc. are selected following earlier applications of this model over this region (e. g. Kumar et al.,  
179 2012; Ojha et al., 2016; Singh et al., 2016; Sharma et al., 2017).

180

## 181 **2.2. Observational data**

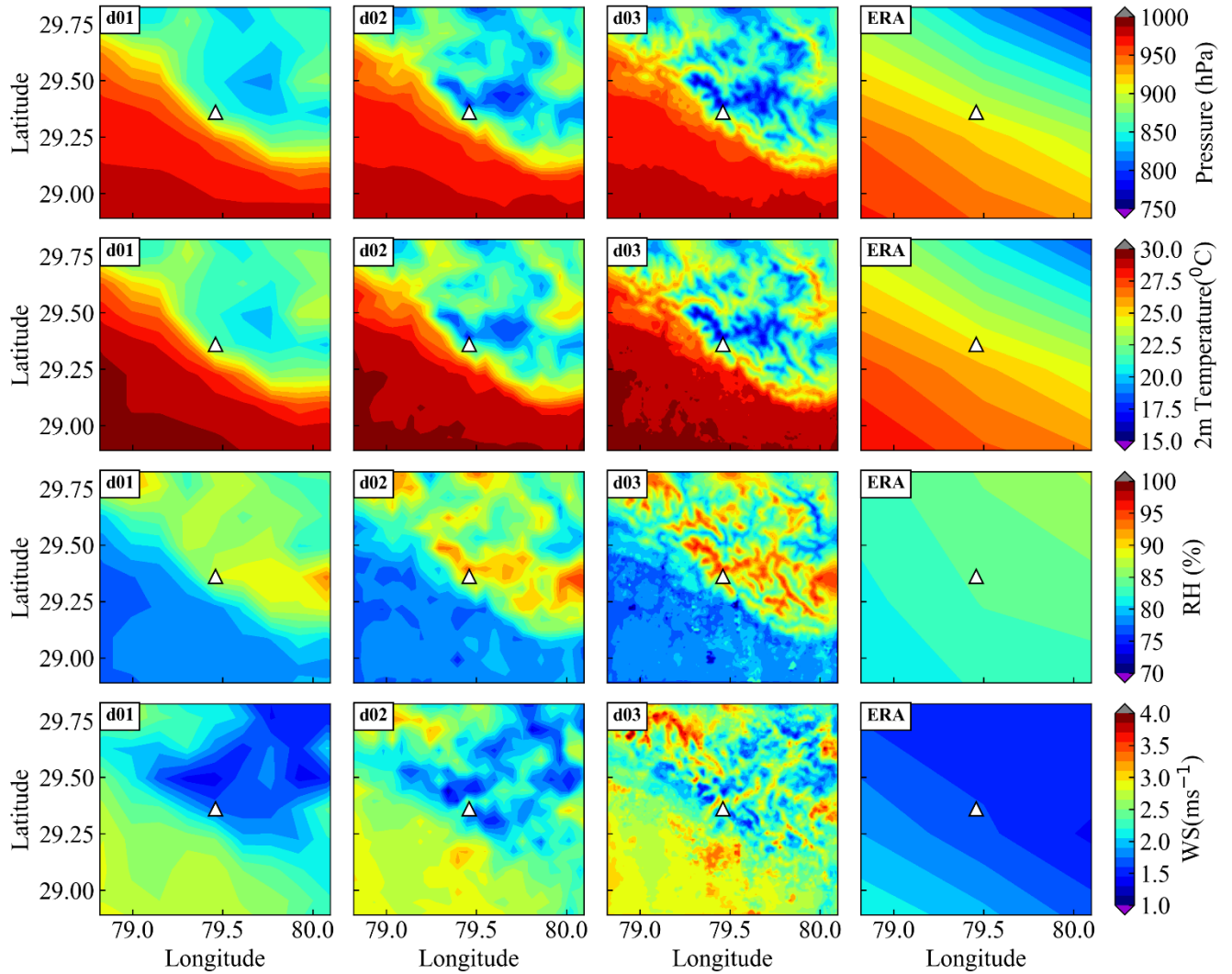
182 We utilize the observations conducted as a part of an intensive field campaign- the Ganges Valleys Aerosol  
183 Experiment (GVAX) for the evaluation of model simulations. The GVAX campaign was conducted using  
184 Atmospheric Radiation Measurement (ARM) Climate Research Facility of the U.S. Department of Energy  
185 (DOE) from June, 10 2011 to March 31, 2012 at ARIES, Manora Peak in Nainital (e.g. Kotamarthi, 2013;  
186 Singh et al., 2016; Naja et al., 2016). The surface-based meteorological measurements of ambient air  
187 temperature, pressure, relative humidity, precipitation, wind (speed and direction) were carried out using  
188 an automatic weather station at 1-minute temporal resolution. **The instantaneous values of the observations  
189 are compared with hourly instantaneous model output at the nearest grid point.**

190 The vertical profiles of temperature, pressure, relative humidity and horizontal wind (speed and direction)  
191 were measured by four launches (00:00, 06:00, 12:00 and 18:00 UTC) of the radiosonde each day during  
192 the campaign (Naja et al., 2016). The continuous vertical profiles of the meteorological parameters except  
193 wind speed and direction were available from end of June 2011 to the entire period of study, whereas valid  
194 wind data were available only for September 2011. Hence, in this study, radiosonde measurements from  
195 July 1, 2011 onwards are used for model evaluation of meteorological parameters, except wind speed and  
196 direction, which are evaluated for the month of September. **A total of 309 valid profiles of temperature  
197 and relative humidity and 104 profiles of wind are used. The statistical metrics mean bias (MB), root mean  
198 square error (RMSE) and correlation coefficient (r) are used for the model evaluation and the description  
199 of these metrics is given in the supplementary material.**

## 200 **3. Results and Discussions**

### 201 **3.1. Comparison with ERA Interim reanalysis**

202 ERA Interim reanalysis data set is available globally at resolution of  $0.75^{\circ} \times 0.75^{\circ}$  with 37 vertical levels  
203 from surface to the top at 1 hPa with covering time period from 1979 to present at 6-hourly time step (Dee  
204 et. al., 2011). Here, we have used the **ERA Interim data available at  $0.75^{\circ} \times 0.75^{\circ}$**  for comparison with  
205 WRF results. We first compare the WRF simulated spatial distribution of meteorological parameters  
206 (surface pressure, 2m air Temperature, 2m RH and 10m WS) with ERA Interim reanalysis over common  
207 area of all the domains and averaged for the complete simulation period (Figure 2). The common area in  
208 all domains includes low-altitude Indo-Gangetic Plain (IGP) region in south (with elevation of less than  
209 400m, Figure 1) and elevated mountains of the central Himalaya in north. Also, for a consistent  
210 comparison, model simulated values are taken at the same time intervals as that in ERA Interim data (i.e.  
211 every 6h). From the comparison Figure 2, it is evident that the meteorological parameters simulated by the  
212 model are dependent on the model grid resolution. The existence of the sharp gradient topographic height  
213 (SGTH) of about 1600 m from the foothill of the Himalaya to the observational site modifies the wind  
214 pattern as well as moisture content differently at different grid resolutions, indicating the critical role of  
215 mountain orography. The surface pressure explicitly depends upon the elevation of a location from mean  
216 sea level. The contour plot of the pressure from ERA Interim shows surface pressure of about 900hPa for  
217 observational site Manora Peak and varied from 550 to 975 hPa within this region, while WRF simulated  
218 pressure is 869 hPa, 835hPa and 827 hPa for d01, d02 and d03, respectively. WRF simulated surface  
219 pressure ranges from 821.9 hPa over high altitude CH region to 977.0 hPa in IGP region within d01. At  
220 the same time, the variation range of surface pressure is 788.1 – 977.5 and 760.4–977.7 hPa within d02  
221 and d03 respectively, and the minimum pressure decreases from d01 to d03 which is attributed to the  
222 improvement in resolved topography on increasing model grid resolution. The effects of the SGTH are  
223 not clearly observed for temperature, wind and RH in ERA-Interim contours, and it could be due to the  
224 unresolved topographic features. Simulated spatial profiles show significantly distinct meteorology in  
225 Indo-Gangetic Plain (IGP), which lies just in the foothills of Himalaya, and elevated central Himalayan  
226 region.



227

228 **Figure 2.** Contours in the first three columns show WRF results for the three domains (first column: d01,  
 229 second column: d02 and third column: d03) and the fourth column shows corresponding parameters from  
 230 the ERA Interim reanalysis. First row shows mean surface pressure during the monsoon (JJAS), second  
 231 row shows 2m temperature (in °C), 3rd row shows 2m relative humidity (RH; %) and bottom row shows  
 232 10 m wind speed (WS; ms<sup>-1</sup>).

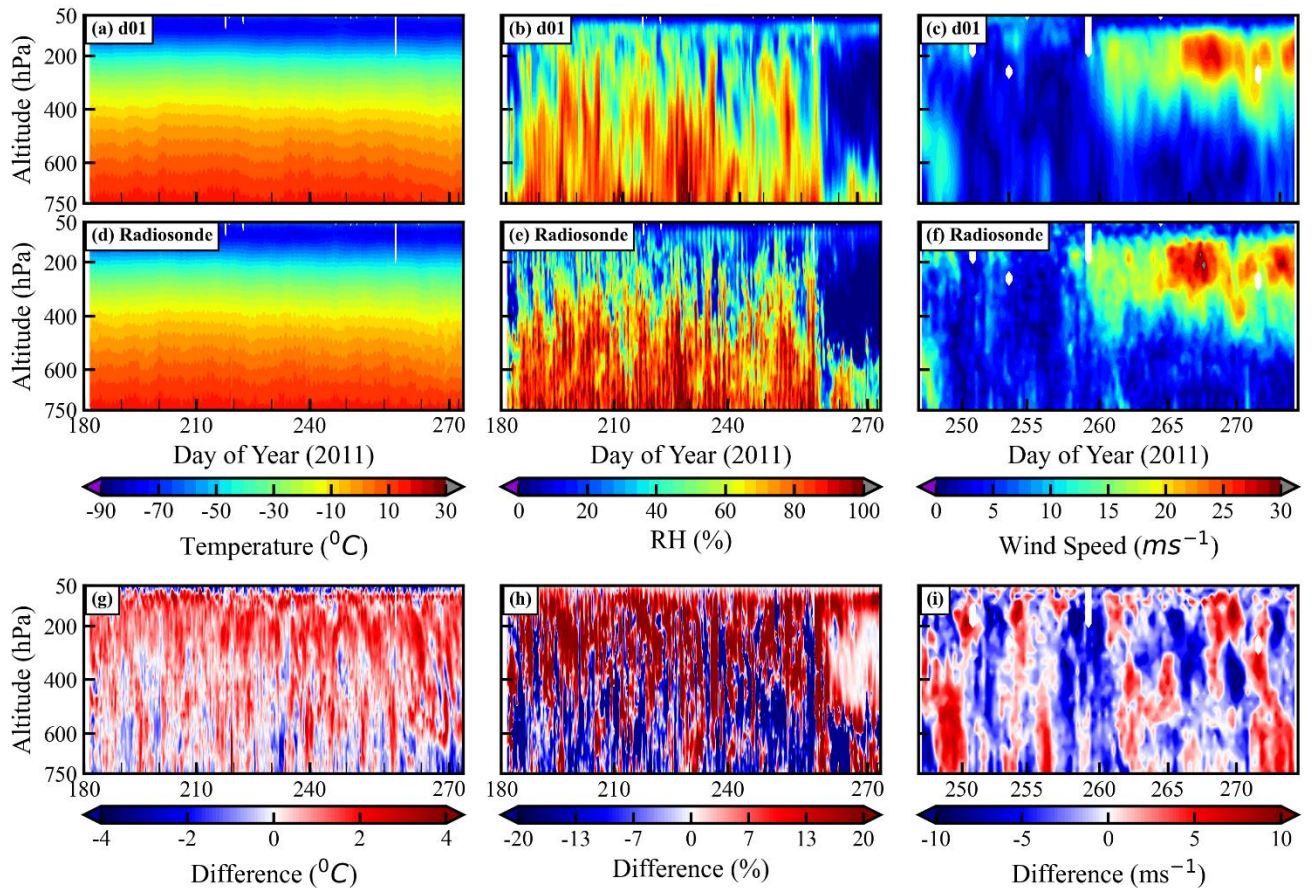
233 The effect of spatial resolution is clearly observed over the mountainous region of Himalaya, where size  
 234 of the mountains changes abruptly, with the modelled output showing distinct features with increasing  
 235 grid resolution. On the other hand, there are minimal differences in the topography of the IGP, and hence  
 236 features are well captured in the model even at coarser resolution of 15 Km.

237 Model simulations show topography dependent spatial variation in the 2m temperature in the ranges of  
238 20.0–29.5°C in d01, 17.3–29.6°C in d02, and 15.5.0–29.9°C in d03 with lowest values simulated over the  
239 elevated mountain peaks and higher values over the temperate IGP region. The contours in three model  
240 domains show explicit dependency of 2m temperature on the grid resolution over the mountainous region.  
241 With increasing model resolution, the topography is resolved to a greater extent and the lower temperature  
242 is simulated at higher surface elevations, as expected. Estimation of water vapour is very important for  
243 both climate and numerical weather prediction (NWP) applications. The relative humidity is above 70%  
244 in all three domains as the study period is monsoon season. The variations (minimum-maximum) in the  
245 relative humidity in ERA-Interim (80% to 85%) data sets, domains d01 (77-93%), d02 (74 – 95%), and  
246 d03 (70- 96%) are generally comparable. The mountain slopes provide the uplift to the monsoonal moist  
247 air that subsequently saturates on ascent and increases the relative humidity to about 90% as observed over  
248 the grid encompassing the site.

249 The wind speed is highly dependent upon the model grid resolution as well as orography-induced  
250 circulations during different seasons (Solanki et al., 2016; Solanki et al 2019) as shown in Figure 2. As  
251 mentioned earlier, although the topography of the IGP region does not vary abruptly, the magnitude of the  
252 wind speed over this region as well as over the complex Himalayan region are found to change  
253 significantly at different model resolutions, thereby indicating that the wind speed is very sensitive to both  
254 model resolution and topography. The wind speed in d01 varies from minimum value of 1.3 ms<sup>-1</sup> to  
255 maximum value of 2.8 ms<sup>-1</sup>, while the wind variations in domains d02 (1.2 – 3.4 ms<sup>-1</sup>) and d03 (1.3 – 4.2  
256 ms<sup>-1</sup>) overestimated as compared to the ERA-interim (1.2–2.3ms<sup>-1</sup>). Overall, the variations in surface  
257 pressure, temperature, and relative humidity are seen to be similar between the two datasets.

### 258 3.2. Comparison with Radiosonde observations

259 Model simulated vertical structure of temperature, relative humidity, and wind speed are evaluated against  
260 the radiosonde observations during the GVAX campaign. Such comparisons from surface to 50 hPa are  
261 shown in the Figure 3a-c for WRF d01 simulation and the radiosonde observations in the Figure 3d-f.

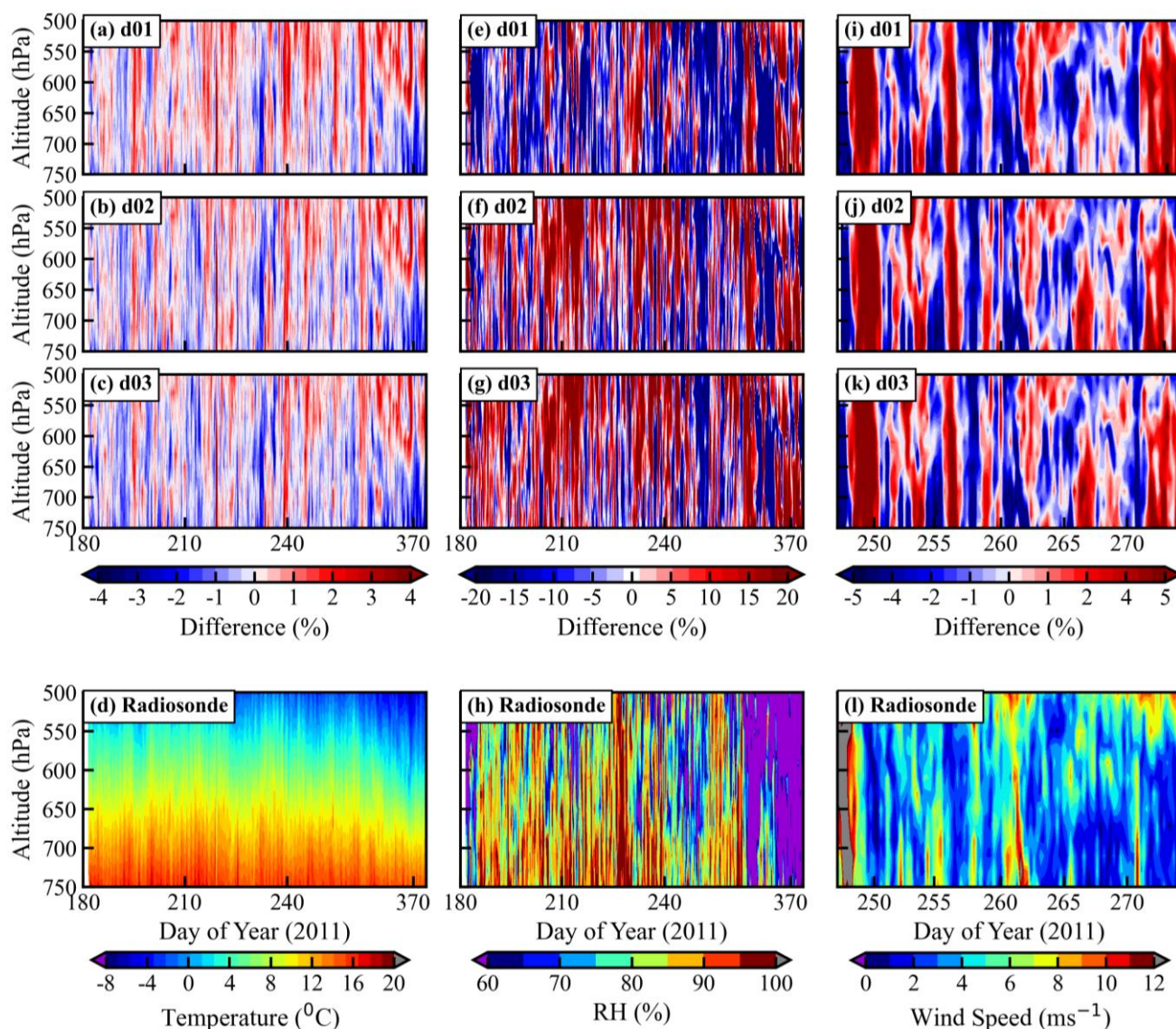


262  
 263 **Figure 3:** The comparison of (a) temperature in  $^{\circ}\text{C}$ , (b) relative humidity (RH; %), and (c) wind speed in  
 264  $\text{ms}^{-1}$  (c) vertical profiles in WRF simulation d01 with the radiosonde observations (d, e, and f). The x-axis  
 265 of (a), (b), (d), (e), (g) and (h) show the day of the year 2011 starting from 1 July (182<sup>nd</sup> day) to 30  
 266 September (273<sup>rd</sup> day). Wind speed profiles (c, f) in  $\text{ms}^{-1}$  are plotted only for month September, 2011. The  
 267 third row (g, h, and i) shows the difference in temperature, relative humidity, and wind speed between  
 268 WRF d01 simulation and radiosonde observation.

269 The inversion of the temperature at the top of the troposphere occurred at  $\sim 90\text{hPa}$  ( $\sim 16\text{km}$ ) in observations.  
 270 Radiosonde profiles (Figure 3a) show that temperature decreases with pressure from  $15.5^{\circ}\text{C}$  at 750 hPa to  
 271  $-78.0^{\circ}\text{C}$  at  $\sim 90$  hPa. Mean temperature profile simulated by the WRF model also captures this variability  
 272 showing a reduction from  $15.1^{\circ}\text{C}$  to  $-76.6^{\circ}\text{C}$  in these pressure levels. Further the difference between  
 273 model (d01) and radiosonde observations (Figure 3g) are found in the range of  $-4$  to  $4^{\circ}\text{C}$ . The mean RH  
 274 values from the radiosonde observation (model d01) also show decrease from 82.3% (76.7%) at 750 to

275 25.2% (32.0%) at 90 hPa. The difference of the mean RH between observation and model (Figure 3h)  
276 shows that model simulates wetter (or more humid) atmosphere at higher altitudes while showing a dry  
277 bias in lower altitudes. The observations of wind speed from radiosonde were available only from 01  
278 September 2011 onwards therefore wind comparison is made only for the September month. The simulated  
279 profiles of the wind agree generally well with the observations. Wind speed is observed less than  $10 \text{ ms}^{-1}$   
280 up to 400 hPa over the month of September and similar magnitude is observed above 400 hPa till mid of  
281 September (day of year 258). Further, the wind speed observed  $\geq 15 \text{ ms}^{-1}$  above 400hPa after 258 day of  
282 year (15 September). The vertical variation of wind speed well simulated by model. For the statistical  
283 comparison of the simulated meteorology with the observations, the Taylor diagram (Taylor, 2001) is used  
284 and shown in Figure 7a. In the diagram the comparison is summarized with correlation coefficient (r),  
285 normalized root mean squared difference (RMSD) and normalized standard deviation (SD), normalized to  
286 the standard deviation of observation. In most of the cases, model simulates less variability in  
287 meteorological parameters as shown by the normalized standard deviation which turns out to be less than  
288 1. For temperature and wind speed, model shows good agreement at 250hPa ( $r > 0.80$ ) than that in lower  
289 altitudes i.e. 750hPa ( $r < 0.40$ ). On the other hand, model captures variability in humidity relatively well  
290 at 500 hPa ( $r = 0.71$ ) but shows poor correlation at 50 hPa ( $r = 0.17$ ) near the model top.  
291 Lower correlations for temperature and wind speed near to the surface (750 hPa) could be due to the terrain  
292 induced effects most significant in the local boundary layer. The, surface level winds, and turbulence etc.  
293 are some of the features of the boundary layer that are largely affected by the surface and terrain  
294 characteristics. The vertical profiles of these parameters for all three model domains only up to 500 hPa is  
295 shown in Figure 4. Differences between the simulated vertical profile of temperature and radiosonde  
296 observation below 500hPa (Figure 4) are in general similar in all the domains. Except for the relative  
297 humidity in d01, other meteorological parameters shown here do not reveal strong dependencies on the  
298 model resolution. Model however overestimates the relative humidity near 500hPa level in d02 and d03

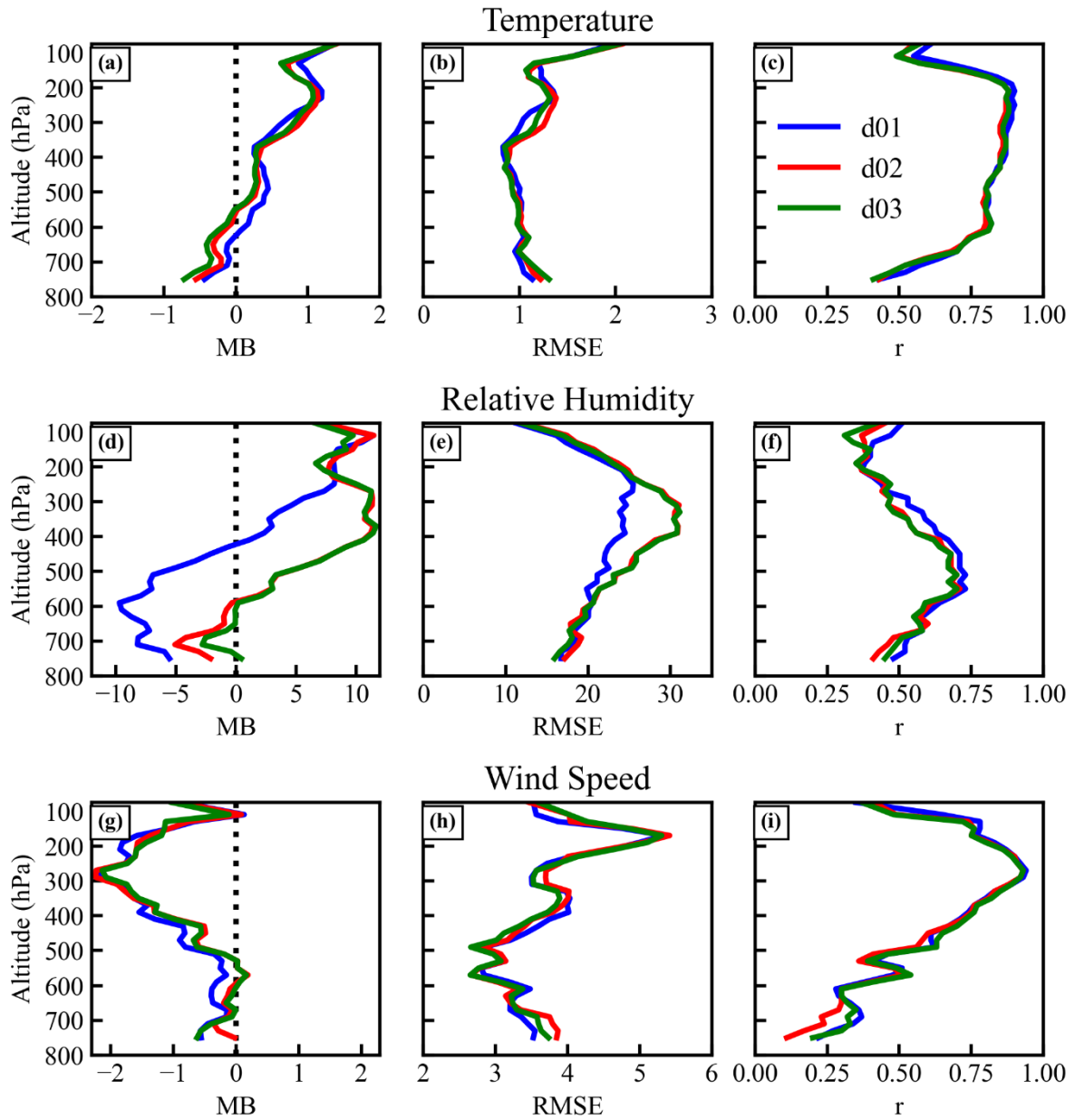
299 on some of the days. In case of the wind speed, the model underestimates the magnitude of the wind in  
 300 first few days up to 500 hPa, though qualitatively the model is able to capture the vertical profiles.



301  
 302 **Figure 4:** Difference between model (d01: first row, d02: second row, d03: third row) and radiosonde  
 303 observation for temperature (first column: a, b, c), relative humidity (second column: e, f, g) and wind  
 304 speed (third column: i, j, k) profiles up to 500 hPa. Radiosonde observations are also shown (fourth row).  
 305 The x-axis of (a-h) shows the day of the year 2011 from 1 July (182<sup>nd</sup> day) to 30 September (273<sup>rd</sup> day).  
 306 Wind speed ( $\text{ms}^{-1}$ ) profiles (i-l) are plotted only for the month September, 2011.

307 Figure 5 shows the vertical profiles of the statistical metrics: mean bias (MB), root mean square error  
 308 (RMSE), and correlation coefficient (r) for temperature, relative humidity, and wind speed for the three

309 simulations (d01, d02, d03). The magnitude of the MB values throughout the troposphere are estimated to  
310 be within about 1 °C, 12 %, 2.5 ms<sup>-1</sup> for temperature, relative humidity, and wind speed, respectively.  
311 Additionally, RMSE values are about 1 °C, 15–30%, and 2.5–5 ms<sup>-1</sup> for temperature, relative humidity,  
312 and wind speed, respectively. As discussed earlier also, correlations between model results and  
313 observations are found to be stronger in the middle and upper troposphere as compared to the lower  
314 troposphere. For temperature, the r values are higher than 0.75 between 600 to 200 hPa, whereas it  
315 decreases up to 0.4 at lower altitudes i.e. near 800 hPa. Correlations in lower troposphere are particularly  
316 weaker (r = ~0.25) in case of wind speed. The results suggest that model captures well the day-to-day  
317 variabilities in the meteorological parameters in the middle upper troposphere and to a minor extent in the  
318 lower troposphere. Relatively weaker correlations in the lower troposphere are suggested to be associated  
319 with more pronounced effects of the uncertainties caused by the underlying complex mountain terrain and  
320 resulting unresolved local effects. Wind fields near the surface have been shown to be strongly impacted  
321 by interactions between terrain and boundary layer besides orographic drag in a modelling study over the  
322 Tibetan Plateau (Zhou et al., 2018) and in measurements over Himalaya (Solanki et al., 2019). Increase in  
323 bias with altitude was reported by Kumar et al (2012) for dew point temperature. Besides the model  
324 physics, the higher uncertainties in radiosonde observations of humidity also contribute to these  
325 differences. The effect of model resolution is not very significant for temperature and wind profiles above  
326 800 hPa, nevertheless, the mean bias in RH is lower in d02 and d03 simulations (~5%) in the 800–600  
327 hPa. Overall, it is seen that model captured the vertical structures of meteorological parameters, however,  
328 better representation of complex terrains itself is insufficient for improving the model performance aloft.  
329 This highlights the need of future studies evaluating various physics schemes on top of better topography  
330 representation considered here. Nevertheless, model biases have been significantly reduced for surface  
331 level meteorology with higher resolution, which is discussed in detail in the next section (3.3).



332

333 **Figure 5.** The vertical profiles of mean bias (MB), root mean square error (RMSE), and correlation  
 334 coefficient (r) for temperature, relative humidity, and wind speed for different domains d01 (blue), d02  
 335 (red) and d03 (green).

336 **3.3. Comparison with ground-based observations**

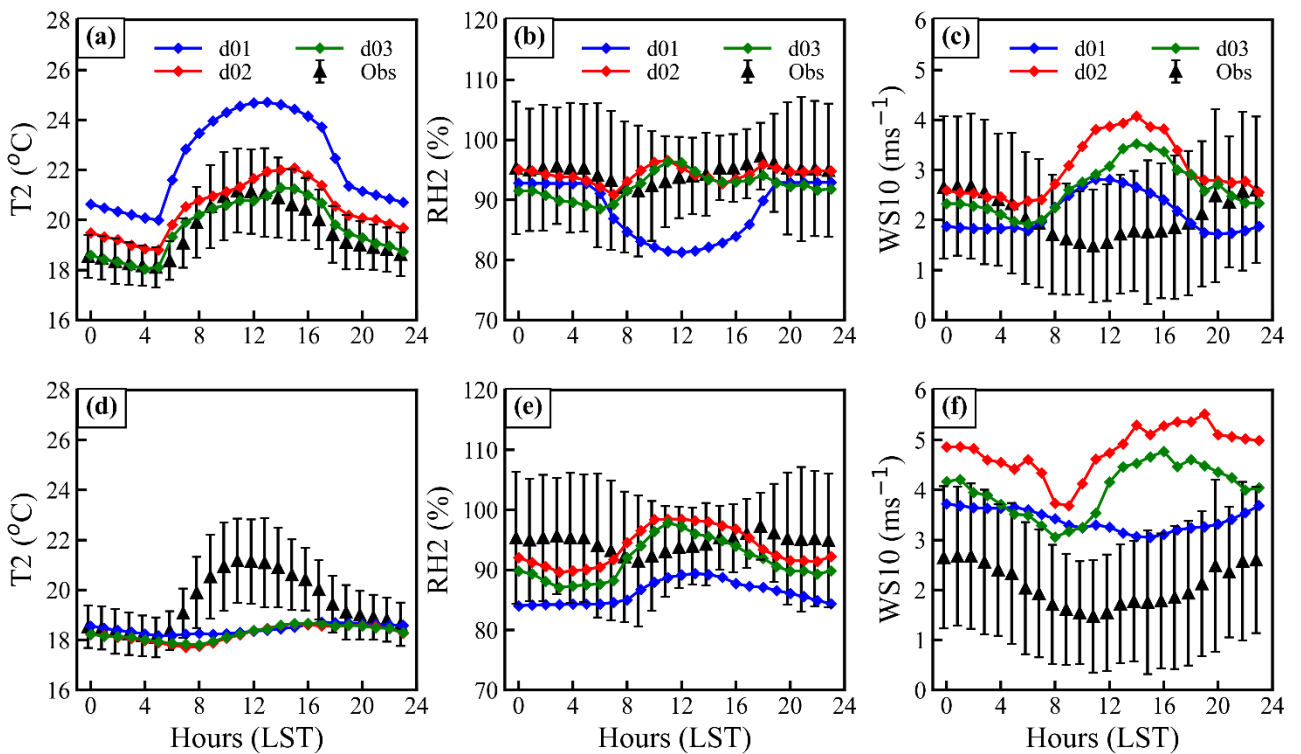
337 Model simulated 2m temperature (T2), 2m relative humidity (RH2) and 10 m wind speed (WS10) for the  
 338 observational site, Manora Peak are compared with the ground-based measurements made during GVAX  
 339 campaign in Figure 6 and summarized in Table1. The diurnal variations in T2, RH2 and WS10 simulated

340 by the WRF model are compared with observations, whereas the surface pressure does not show a  
341 significant diurnal variation (not shown here). Model simulation d01 shows a positive bias of 68 hPa in  
342 surface pressure with strong correlation ( $r = 0.97$ ) with observation (mean =  $\sim 801$  hPa). A significant  
343 improvement is achieved (MB = 26 hPa) in d03 i.e. the finest resolution simulation (Figure 6b and Table  
344 1). WRF model simulated T2 shows warm bias in all the three domains. The simulated T2 for d01 varies  
345 from 16.2 to 28.7  $^{\circ}\text{C}$  with the higher mean value of  $22.3 \pm 2.1^{\circ}\text{C}$  compared to observed mean value of about  
346  $19.5 \pm 1.6^{\circ}\text{C}$  with a correlation of  $r = 0.75$  between d01 and observation. This warm bias is seen to decrease  
347 from d01 (2.8  $^{\circ}\text{C}$ ) with increasing model resolution to 0.2 $^{\circ}\text{C}$  in the d03 simulation (Table S1). The mean  
348 value of the RH2 in d01 is about 88.2 $\pm$ 9.7% lower by 6.4% lower than the observed value 94.7 $\pm$ 9.5% with  
349 the correlation about 0.45 (Figure 7bs). MB and RMSE values of RH2 show a decrease with increasing  
350 model resolution (Table S1). As relative humidity also depends on temperature therefore the diurnal  
351 variation in 2m specific humidity (Q2;  $\text{g kg}^{-1}$ ) has also been analyzed (Figure S1). Q2 is observed in the  
352 range of 5.5–21.5  $\text{g kg}^{-1}$  with mean value as  $16.8 \pm 2.0 \text{ g kg}^{-1}$ . It is found that the agreement in Q2 is  
353 relatively better (MB = -0.7;  $r = 0.77$  in d03), when the statistical metrics are compared with that for RH  
354 (Table S1). The wind speed plays a vital role in transport processes and controls the dynamics of the  
355 atmosphere at different temporal and spatial scales. The average 10m wind speed (WS10) over the  
356 measurement station is about  $2.1 \pm 1.4 \text{ ms}^{-1}$  which is similar in d01 ( $2.1 \pm 1.1$ ) while overestimated in d02  
357 by  $0.9 \text{ ms}^{-1}$  and  $0.5 \text{ ms}^{-1}$  d03 (Table 1 and Table S1). The correlation in case of the WS10 is 0.18 in d01  
358 and d02 which improves to 0.24 in d03. The diurnal variation of WS10 (Figure 6c) is not well captured  
359 especially during the noontime.

360 **Table 1:** Mean values along with minimum and maximum of the meteorological parameters: surface  
361 pressure (P; hPa), 2m Temperature (T2;  $^{\circ}\text{C}$ ); 2m relative humidity (RH2; %) and 10m wind speed (WS10;  
362  $\text{ms}^{-1}$ ) in the model simulations and observations. An additional evaluation is presented accounting for the  
363 difference in model surface altitude and actual altitude of measurements (referred to as with altitude  
364 adjustment).

Parameter	Without altitude adjustment			With altitude adjustment			Observation
	d01	d02	d03	d01	d02	d03	
P (hPa)	869.6±2.6	835.3±2.5	827.6±2.4	801.3±2.4.6	801.3±2.4	801.4±2.4	801.1±2.4
Min/Max	862.8/875.1	828.3/840.8	821.2/833.1	795.0/806.7	795.0/806.7	795.2/806.8	795.1/806.8
T2 (°C)	22.3±1.8	20.4±1.8	19.8±1.1	18.4±0.8	18.4±0.9	18.3±0.9	19.5±1.1
Min/Max	16.2/28.7	15.1/26.0	14.0/25.0	16.1/20.9	15.5/21.8	15.6/22.1	14.8/25.6
RH2(%)	88.2±9.7	94.3±6.4	92.3±7.9	86.2±10.9	93.8±8.5	91.5±9.7	94.7±9.5
Min/Max	53.3/100	67.6/100	52.3/100	43.9/100	51.3/100	47.9/100	31.6/100
WS10 (ms <sup>-1</sup> )	2.1±1.1	3.0±1.4	2.6±1.7	3.4±2.6	4.8±3.1	4.0±3.1	2.1±1.4
Min/Max	0.0/8.6	0.1/11.4	0.1/11.7	0.0/20.2	0.1/23.9	0.1/22.1	0.0/10.0

365



366

367 **Figure 6:** Mean diurnal variations of (a) 2m temperature: T2, (b) 2m relative humidity: RH2, and (c) 10m  
 368 wind speed: WS10 from model simulations (d01, d02 and d03) and observations. Altitude adjusted  
 369 variations are also shown (d-f).

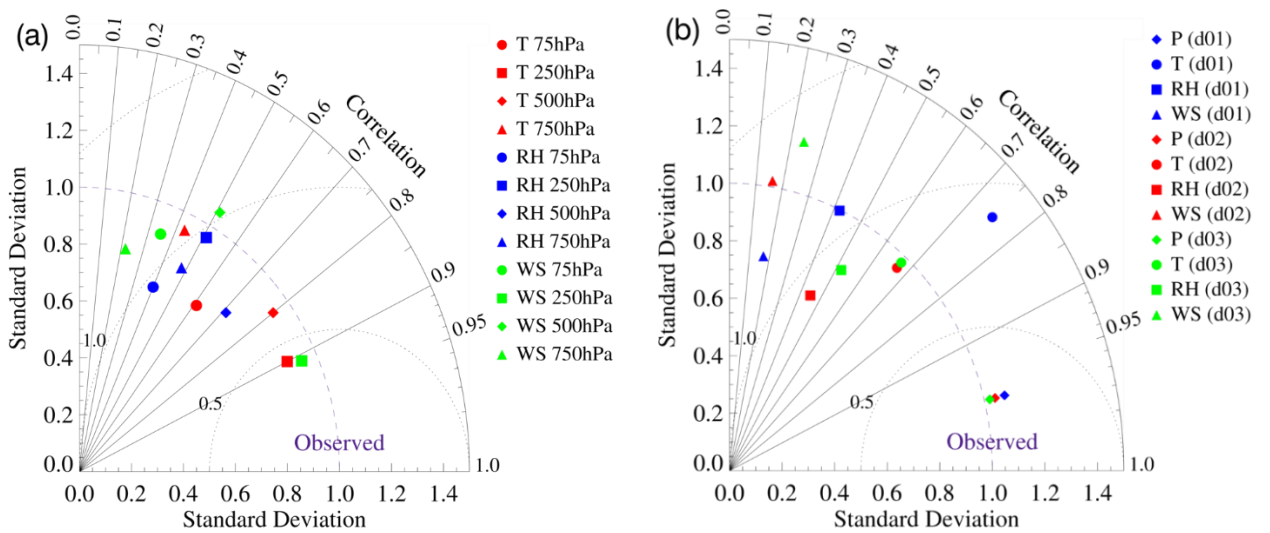
370

371 Due to the complex terrains and the grid size of the model, the simulated altitude of the station could differ  
372 from the reality. In this study, the model underestimated station altitude by about 588m, 480m, and 270m  
373 in d01, d02, and d03 respectively. We performed an additional evaluation to explore how much  
374 improvement can be achieved by linearly interpolating the vertical profile of meteorological parameters  
375 to the actual altitude of the station (Figure d-f), as done in few previous studies (e.g. Mues et al., 2018).  
376 Analysis shows that correlations between model and observations do not show a clear improvement (e.g.,  
377 T2: 0.35) by adjusting the altitude in model output except in case of WS10. Additionally, variability in  
378 temperature is not captured by the model over diurnal (Figure 6 a, d) as well as the day to day timescales  
379 i.e.  $r$  drops from 0.67 to 0.36 in d03 after the adjustment of altitude. As expected the altitude adjustment  
380 does reduce bias in pressure. Nevertheless, reductions in mean biases are not achieved (Table S1), instead,  
381 absolute values of biases show increase from 0.2 to 1.2, 2.4 to 3.1, 0.5 to 1.9, 0.7 to 1.6 in T2, RH2, WS10,  
382 and Q2 in simulation d03. Besides thermal and mechanical interactions of the mountain surfaces with  
383 atmosphere, local processes such as the evaporation, transpiration, etc. affect meteorological conditions in  
384 the air just above the surface. A reduction in wind speed during the daytime is associated with the  
385 competing effects of mountain-valley circulation due to the heating of the slopes versus synoptic-scale  
386 flow (Solanki et al., 2019). To resolve such sub-grid scale processes, we emphasize that very high-  
387 resolution simulations are needed, such as conducted here, to simulate in a satisfactory way the  
388 meteorological variability. The analysis further highlights a need of accurate representation of the complex  
389 topographical features rather than altitude adjusted estimations which lead to very limited improvements.  
390 Here onwards we will discuss the evaluation without altitude adjustment until stated otherwise.

391 We evaluate the MB values in model simulations considering the benchmarks as suggested by Emery et  
392 al. (2001). In the d03 simulation, MB values for both T2 (0.2<sup>0</sup>C) and Q2 (-0.7) are found to be well within  
393 the range of benchmark values:  $\pm 0.5^{\circ}\text{C}$  for T2 and  $\pm 1.0 \text{ g kg}^{-1}$  for Q2. It is important to note that biases in  
394 T2 in the coarser simulations d01 (2.8<sup>0</sup>C) and d02 (0.9<sup>0</sup>C) are however higher as compared to the  
395 benchmarks. MB values in T2 estimated here for the Himalaya are found to be slightly lower (+0.2) (-1.2

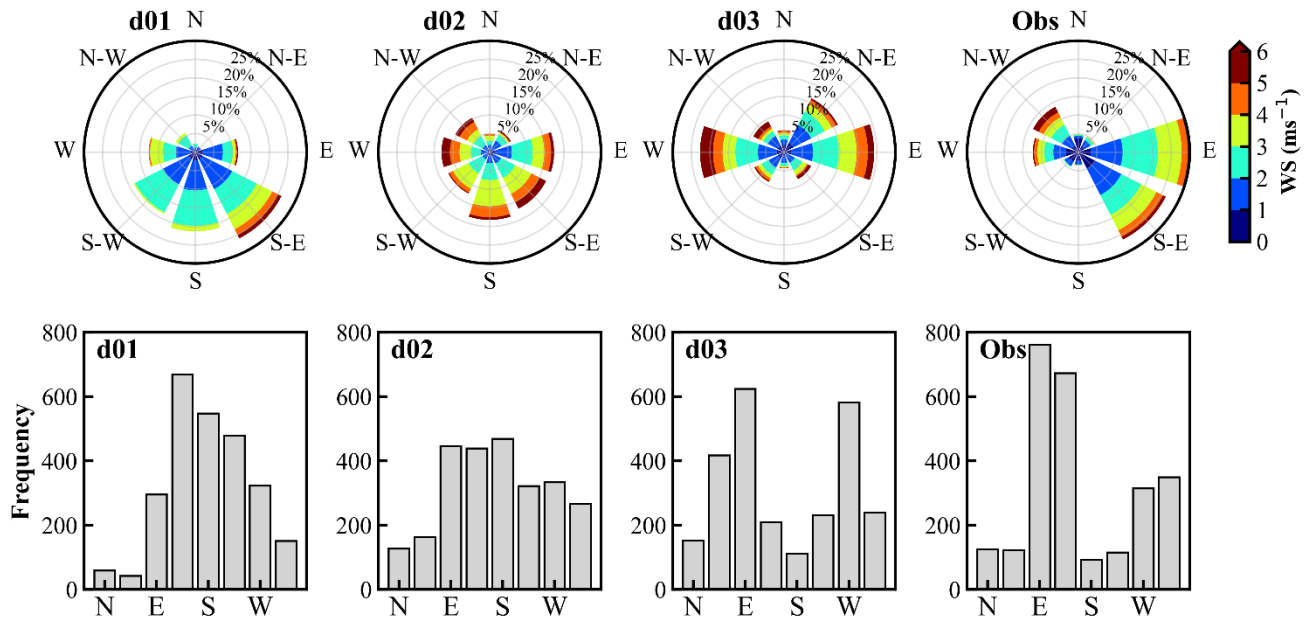
396 with altitude adjustment) than that over the Tibetan Plateau (-2 to -5) (Gao et al., 2015) and over  
 397 mountainous regions in the Europe (Zhang et al., 2013). Warmer bias in our case is due to underestimation  
 398 of Himalayan altitude, whereas, model overestimated terrain height over the Tibetan Plateau region giving  
 399 contrasting results. Further, the RMSE in wind speed here is lower ( $1.6\text{--}2.0\text{ ms}^{-1}$ ) than that over  
 400 Kathmandu valley ( $2.2\text{ ms}^{-1}$ ; Mues et al., 2018) and similar to benchmark ( $2.0\text{ ms}^{-1}$ ). Mar et al. (2016) also  
 401 reported similar bias ( $2\text{ ms}^{-1}$ ) in the 10m wind speed over Europe and average correlation of  $\sim 0.4\text{--}0.6$  over  
 402 the Alps. As also seen here, simulating near surface diurnal winds remains challenging over complex  
 403 terrains, although the bias was reduced after including effects of the turbulent orographic form drag (Zhou  
 404 et al., 2017; 2019). Besides turbulent orographic form drag, it is suggested that wind speed is sensitive  
 405 towards boundary layer schemes (Yver et al., 2013; Zhou et al., 2019) and that more studies are needed to  
 406 explore these aspects over the central Himalaya.

407



408

409 **Figure 7:** Taylor diagram with correlation coefficient, normalized standard deviation, and normalized root  
 410 mean square difference (RMSD) error for (a) model performance at different pressure levels shown in  
 411 Figure 3 for d01, and (b) the model simulated surface pressure, 2m temperature, RH and 10 m wind speed  
 412 for different domains as shown in Figure 6a-c.



413

414

415 **Figure 8:** Comparison of the wind speed and direction as shown in form of wind rose (top panel), and  
 416 frequency distribution of wind direction (bottom row) from model simulations over the three domains  
 417 (d01, d02, d03) and observations (obs) during June-September 2011. Different colours and radius of wind  
 418 roses show the wind speed and frequency of counts respectively.

419

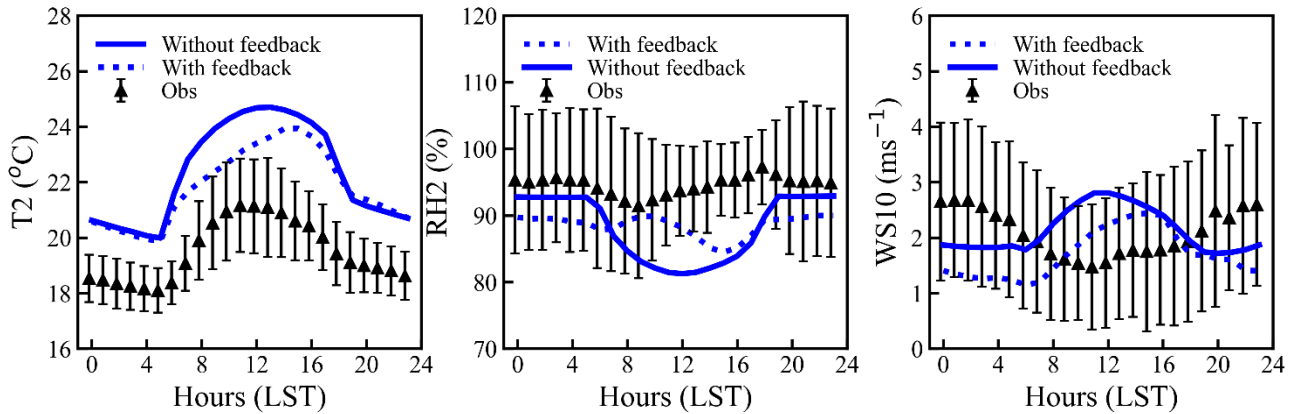
420 The wind direction is strongly influenced by the surrounding topography over the mountainous region and  
 421 the evaluation of the wind direction at horizontal resolution is shown Figure 8. The winds varying between  
 422 meteorological direction  $337.5^{\circ}$  to  $22.5^{\circ}$  are considered to be the Northerly and represented by N in the  
 423 frequency distribution and so on for other directions taking into account the clockwise meteorological  
 424 convention. The dominance of the wind flow over the observational site is easterly (30%) and south  
 425 easterly (26%) while 26% wind flows from the west and north-west. The frequency of southerly (539) and  
 426 south-westerly (SW, 481) are quite higher in d01 as compared to the observations (93 and 118  
 427 respectively), which decreases up to 109 and 232 in d03. Model is able to simulate the northerly and north-  
 428 easterly winds in d01 and d02, while, model simulates larger contribution of north easterly winds in d03

429 which is not present in the observations. The dominance of the summer monsoon seasonal easterly (30%)  
430 and south-easterly (27%) winds are clearly seen in the observation. The easterly component of the model  
431 simulated wind shows better agreement with observations on increasing the model resolution.  
432 Additionally, the model is able to simulate the westerly and north-westerly wind contribution in d02,  
433 whereas, the westerly component is over predicted by 10% in d03. The winds blowing from north, north-  
434 easterly, south and south-westerly are very weak ( $<2\text{ms}^{-1}$ ) and are about ~15% of the total winds. **Wind**  
435 **direction changed during transitions from high to low wind conditions during morning hours (7–10 h), and**  
436 **then low to high during evening (18–20 h). Overall, the simulated wind field in d03 are relatively in better**  
437 **agreement with observations than that of d01 and d02. This is further assessed in the section 3.5 using a**  
438 **finer resolution simulation through implementation of SRTM 3s terrain data.**

439

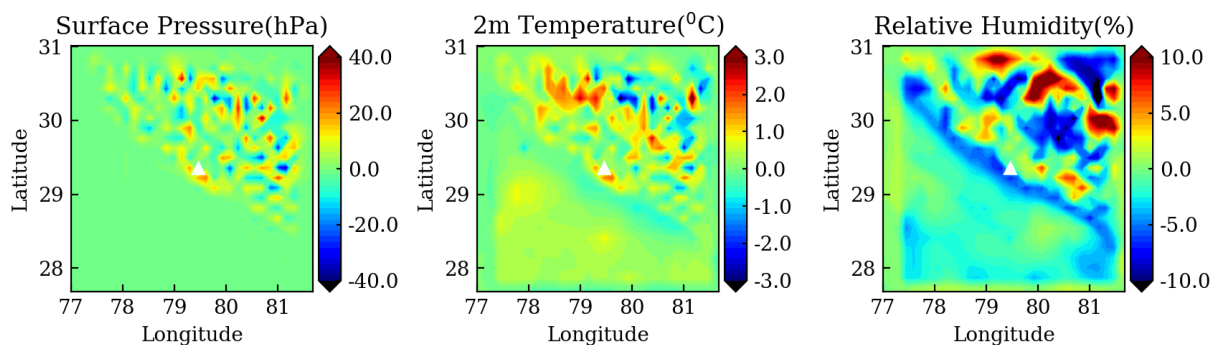
#### 440 **3.4. Effect of feedback**

441 In the preceding section, the results of the simulations carried out without any feedbacks (WRF-WF) from  
442 the finer resolution domain to its parent domain were presented. This WRF-WF experiment was conducted  
443 in such a way that it could explicitly account for the grid resolution effects on the model performance. The  
444 simulated meteorology with this model setup depicted different model performance in outermost coarse  
445 resolution domain d01 as compared to d02 and d03 (Figure 2 and 6). The model performance depends  
446 upon the boundary and initial conditions. Another model simulation is carried out in this section using the  
447 same configuration but with two-way interactive nesting and feedback (WRF-F) from daughter domain to  
448 its parent domain. The simulated meteorological parameters in higher nest are fed back to its parent  
449 domains and the boundary conditions replaced there. The model results over CH region in the regional  
450 scale simulation (d01) shows better agreement with the observations because of the feedback from high  
451 resolution nested simulation. The comparison of the simulated meteorological parameters (T2, RH2, and  
452 WS10) for outermost domain with the surface observations is presented in Figure 9 for both WRF-WF  
453 and WRF-F, and the effect of the feedback within outermost domain.



454 **Figure 9:** Diurnal variation of the T2, RH2, and WS10 from d01 without feedback (WRF-WF) and with  
 455 feedback (WRF-F) simulations.

456 The comparison of mean values (Table 2) shows a decrease in model bias for T2, RH2, and Q2 by 0.5 °C,  
 457 0.3%, and 0.2 gkg<sup>-1</sup> respectively due to feedback from finer resolution simulations. Additionally,  
 458 correlations are found to be improved for RH2 and Q2 by 0.15 and 0.12 respectively due to feedback.  
 459 Nevertheless, smaller changes were seen in correlations for WS10 (by 0.05) and T2 (by -0.02) (Figure S2).  
 460 Variations in wind speed and direction shows an improvement in dominant flow direction e.g. easterly,  
 461 westerly and north-westerly (Figure S3). Effects of the feedback on surface pressure, T2, and RH2 at over  
 462 domain d01 is shown in Figure 10. Feedback effects is seen to be more pronounced over mountainous  
 463 region than over the plain region of IGP.



464  
 465 **Figure 10:** The effect of the two-way nesting on d01 is shown. The difference between the simulations  
 466 with feedback (WRF-F) and without feedback (WRF-WF) is shown for surface pressure, 2m temperature,  
 467 and 2m relative humidity.

468 **Table 2:** Comparison of the simulated meteorology for surface pressure (P), 2m Temperature (T2), 2m  
 469 relative humidity (RH2), 10m wind speed (WS10) and 2m specific humidity (Q2) in two model  
 470 simulations: WRF-WF and WRF-F at the observational site from outermost domain d01.

Parameters	Observed	WRF-WF	WRF-F
P (hPa)	801.4±2.4	869.6±2.6	858.9±2.5
T2 (°C)	19.5±1.6	22.3±2.1	21.9±1.4
RH2 (%)	94.7±9.5	88.2±4.9	88.6±4.9
WS10 (ms <sup>-1</sup> )	2.1±1.4	2.1±1.1	1.7±1.3
Q2(g kg <sup>-1</sup> )	16.8±2.0	17.3±2.0	17.0±2.1

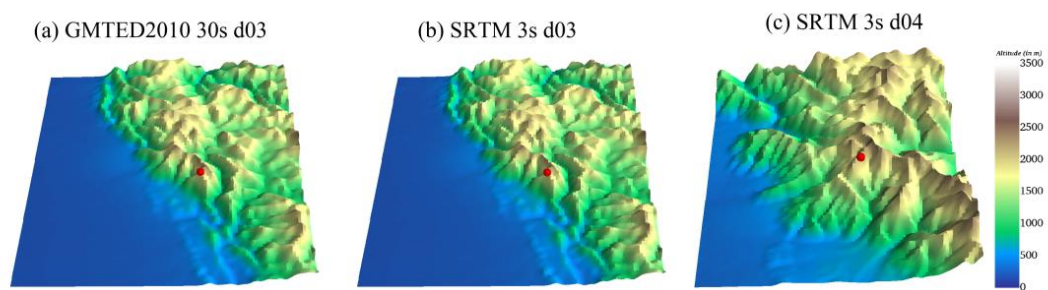
471

472 The feedback from the daughter domain to parent domain process mostly modifies the meteorology over  
 473 the mountainous region within the domain. The effect of feedback is strikingly observed for the 2m  
 474 temperature and the trend of diurnal variation of the relative humidity. **The analyses of biases and  
 475 correlations suggest an improvement in the model simulated pressure, temperature, and humidity through  
 476 feedback from well resolved nests. This further underpins that better representations of Himalaya over  
 477 local-scales can be adopted to simulate meteorology over regional-scale with lower biases over complex  
 478 terrains in the domain.** Nevertheless, further modelling studies alongside with more observations are  
 479 needed to improve the model performance. We make further effort on the improvement of the wind speed  
 480 and direction over the complex topography by implementing a high resolution (3s) topographical input in  
 481 the model to evaluate further fine resolution features over Himalaya in the next section.

### 482 **3.5. Inclusion of high resolution (3s) SRTM topography**

483 Simulations described in previous sections were performed using the 30s (~1km) topographic data from  
 484 the GMTED2010 (Danielson and Gesch, 2011). The resolution of this (30s or ~0.95km) is comparable to  
 485 the highest resolution of the WRF simulation (d03). To evaluate influences of topographical features

486 over even finer scales on the wind flows over this highly complex terrain, topography input available at  
 487 very high resolution (3s or ~90m) from the Shuttle Radar Topography Mission (SRTM3s) (Farr et al.,  
 488 2007) has been implemented without altering the model configuration, except performing the simulation  
 489 as d04 (~333m). Simulation with SRTM data at 1 km resolution did not differ significantly with the  
 490 similar resolution simulation using GMTED2010 (GMTED hereinafter). For this experiment, model  
 491 simulation is performed for 1 month only (September 2011). This simulation carried out without  
 492 feedback and compared with the observation to check the effect of implementing high-resolution  
 493 topography.

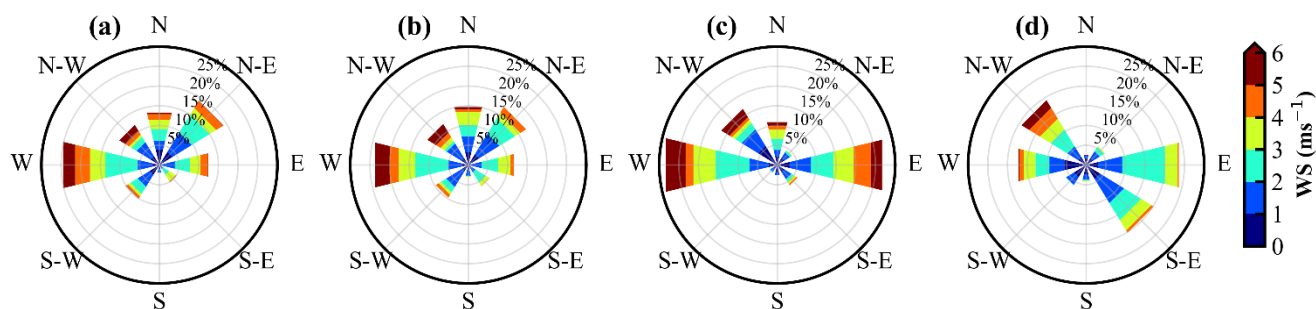


Red dot reperests observatinal site Manora Peak

494  
 495 **Figure 11:** The topography from GMTED at 30s and SRTM at 3s in domain d03 and d04.

496  
 497 The differences of the topographic height between GMTED and SRTM3s as shown in Figure S4 shows  
 498 that the differences are larger over the mountainous region which varies from -100 to +100m. The  
 499 differences are lower in within d02 and d03 by changing input from GMTED to SRTM3s. The topography  
 500 in the d04 get better resolved as depicted by sharp variations of mountain ridges and valleys using the  
 501 SRTM3s as compared to the d03, as shown in the Figure 11, which could be smoothed out if the simulation  
 502 was carried out with GMTED / or at 1 km with SRTM3s. The induced effects due the more resolved  
 503 variability of topographic height in d04 can better simulate the local circulation of air mass. **After including**  
 504 **the SRTM3s topography, the MB and RMSE values for wind speed in d03 reduced slightly (~0.04 ms<sup>-1</sup>).**  
 505 **Additionally, wind directions also improved by ~1–2% for different directions after using the SRTM3s.**  
 506 Therefore, simulated 10 m wind direction in d04 is compared with the observations and d03 to investigate

507 the effect of including the SRTM3s topography. Surface pressure is seen to be simulated more realistically  
 508 (809 hPa) and the dry bias in 2m relative humidity is improved by ~2%. Simulations of diurnal wind  
 509 variations remain challenging (not shown here) even at finest resolutions considered here (d04) with  
 510 updated topographic data (SRTM3s). The variations in winds are analysed by wind rose (Figure 12) and  
 511 frequency distribution (Figure S5). A comparison is performed between d03 before and after using  
 512 SRTM3s and the innermost nest d04 with SRTM3s. The fraction of north-easterly component in d04 with  
 513 SRTM3s (5%) is found to be comparable to observation (6%), which was overestimated 19% (17%) in  
 514 d03 with GMTED (SRTM3s). The southerly wind component consistently shows an agreement with the  
 515 observations with increasing model resolution. The observation shows the prevalence of north-westerly  
 516 (19%), easterly (24%), westerly (18%) and south-easterly (20%) winds and these are also seen to be  
 517 dominant directions in the simulation d04, while occurrence of south-easterly winds is underestimated.



518  
 519 **Figure 12:** Wind roses (a) d03 using GMTED, (b-c) d03 and d04 using SRTM3s topography data, and (d)  
 520 surface observation. The comparison of the wind speed and direction shown for the month September,  
 521 2011.

522 Simulation of the wind directions improved from d03 to d04 by using the SRTM3s topography being  
 523 relatively in better agreement with observations, except certain wind directions such as south easterly. An  
 524 improvement is noticed in simulated surface pressure, 2 m relative humidity and 10 m wind speed using  
 525 the SRTM3s topography over the complex CH. The impact of the orographic variation with different  
 526 resolution topographic data in RH (Figure S6) shows the differences are in range of -1 to 1% in d02 and -

527 3% to 3% in d03. Such variations are due to inclusion of the SRTM3s high resolution topographic data.  
528 Such multi-scale orographic variations are found to be key factors in meteorological simulation over  
529 complex terrains (e.g. Wang et al., 2020). The effects of the SRTM3s topographic static data is studied  
530 previously over other regions of the world (e. g. Teixeira et al., 2014; De Meij and Vinuesa, 2014).  
531 However, the daytime lower wind speed and the transition phases during morning and evening hours still  
532 remain a challenge even after using the high resolution (333m x 333m) nest. Such discrepancies between  
533 model and observations over the Himalayan region are suggested to be associated with still unresolved  
534 terrain features, besides the influences of input meteorological fields as well as the model physics on  
535 simulated atmospheric flows (e. g. Xue et al., 2014; Vincent et al., 2015).

536

#### 537 **4. Summary and Conclusions**

538 In this study, the effects of spatial resolution on model simulated meteorology over the CH has been  
539 examined combining the WRF model with ground-based, balloon-borne observations during and intensive  
540 field campaign, and reanalysis datasets. Owing to the highly complex topography of the central Himalaya,  
541 model results show strong sensitivity towards the model resolution and adequate representation of terrain  
542 features. Model simulated meteorological profiles do not show much dependency on resolution except in  
543 the lower atmosphere, which is directly influenced by terrain induced effects and surface characteristics  
544 emphasizing the need also to evaluate various physics schemes over this region. The biases in 2 m  
545 temperature, relative humidity and pressure show a decrease on increasing the model resolution indicating  
546 a better resolved representation of topographical features. Diurnal variations in meteorological parameters  
547 also show better agreements on increasing the grid resolution. Although the surface pressure does not  
548 show a pronounced diurnal variation nevertheless the biases in simulated surface pressure reduce  
549 drastically over fine resolution simulations. Interpolation of coarser simulations (d01, d02) to the station  
550 altitude reduces the bias in surface pressure and temperature, but suppresses the diurnal variability. The  
551 results highlight the significance of accurately representing terrains at finer resolutions (d03). Model is

552 generally not able to reproduce the wind directions well, except some of the major components in all the  
553 simulations with varying resolutions. The directionality of the simulated winds show improvements over  
554 finer grid resolutions nevertheless reproducing the diurnal variability remains a challenge. Biases are  
555 stronger typically during daytime and also during transitions of low to high wind conditions and vice versa.  
556 This is attributed to the uncertainties in representing the interaction of slope winds with synoptic mean  
557 flow and local circulations, despite of an improved representation of terrain features. A sensitivity  
558 experiment with domain feedback turned ON shows that the feedback process can improve the  
559 representation of the CH in the simulation covering larger region of the northern Indian subcontinent. It is  
560 suggested that further improvements in the model performance are limited due to the lack of high-  
561 resolution topographical inputs biases through input meteorological fields, and model physics.  
562 Nevertheless, an implementation of a very high resolution (3s) topographical input using the SRTM data  
563 shows potential to reduce the biases related to topographical features to some extent.

564

#### 565 **Code and data availability**

566 Observational data from the GVAX campaign is available freely  
567 (<https://adc.arm.gov/discovery/#v/results/s/fsite::pgh.M>). WRF is an open-source and publicly available  
568 model, which can be downloaded at [http://www2.mmm.ucar.edu/wrf/users/download/get\\_source.html](http://www2.mmm.ucar.edu/wrf/users/download/get_source.html).  
569 A zip file containing a) namelists for both pre-processor (WPS) as well as the WRF, b) 3 s resolution  
570 topography input prepared for the pre-processor, along with a README file describing details necessary  
571 to perform the simulations, has been archived at <https://doi.org/10.5281/zenodo.3978569>.

572

#### 573 **Author contributions**

574 NS and AP designed and supervised the study. JS performed the simulations, assisted by NO and AS. JS,  
575 NO, AS analysed the model results and NVPKK, KR, SSG contributed to the interpretations. VRK

576 contributed significantly in conceiving and realizing the GVAX campaign. JS and NS wrote the first draft,  
577 and all the authors contributed to the manuscript.

578

## 579 **Acknowledgement**

580 This study has been supported by ABLN& C: NOBLE project under ISRO-GBP. We are thankful to  
581 Director ARIES, Nainital. We acknowledge NCAR for the WRF-ARW model, ECMWF for the ERA-  
582 Interim reanalysis data sets, ARM Climate Research Facility of U.S. Department of Energy (DOE) for  
583 availing the observations made during GVAX campaign. Computing resources from the Max Planck  
584 Computing and Data Facility (MPCDF) are acknowledged. N. Ojha acknowledges the computing  
585 resources - Vikram-100 HPC at Physical Research Laboratory (PRL), and valuable support from  
586 Duggirala Pallamraju and Anil Bhardwaj. **Constructive comments and suggestions from the anonymous  
587 reviewers and the handling editor are gratefully acknowledged.**

588

## 589 **References**

590 Bhutiyani, M.R., Kale, V.S. and Pawar, N.J.: Long-term trends in maximum, minimum and mean annual  
591 air temperatures across the Northwestern Himalaya during the twentieth century. Climatic Change, 85, 59-  
592 177, <https://doi.org/10.1007/s10584-006-9196-1>, 2007.

593 Bonasoni, P., Cristofanelli, P., Marinoni, A., Vuillermoz, E. and Adhikary, B.: Atmospheric pollution in  
594 the Hindu Kush–Himalaya region: Evidence and implications for the regional climate. Mountain research  
595 and development, 32, 468-479, 2012.

596 Boyle, J. and Klein, S.A.: Impact of horizontal resolution on climate model forecasts of tropical  
597 precipitation and diabatic heating for the TWP-ICE period. Journal of Geophysical Research:  
598 Atmospheres, 115, <https://doi.org/10.1029/2010JD014262>, 2010.

599 Caya, D. and Laprise, R.: A semi-implicit semi-Lagrangian regional climate model: The Canadian RCM.  
600 Monthly Weather Review, 127, 341-362, [https://doi.org/10.1175/1520-  
601 0493\(1999\)127<0341:ASISLR>2.0.CO;2](https://doi.org/10.1175/1520-0493(1999)127<0341:ASISLR>2.0.CO;2), 1999.

602 Chen, F. and Dudhia, J.: Coupling an advanced land surface–hydrology model with the Penn State–NCAR  
603 MM5 modeling system. Part I: Model implementation and sensitivity. *Monthly Weather Review*, 129,  
604 569–585, [https://doi.org/10.1175/1520-0493\(2001\)129<0569:CAALSH>2.0.CO;2](https://doi.org/10.1175/1520-0493(2001)129<0569:CAALSH>2.0.CO;2)2001.

605 Cheng, W. Y. Y. and Steenburgh, W. J.: Evaluation of surface sensible weather forecasts by the WRF and the Eta  
606 Models over the western United States, *Weather Forecast.*, 20(5), 812–821, doi:10.1175/WAF885.1, 2005.

607 Chou, M.D. and Suarez, M.J.: An efficient thermal infrared radiation parameterization for use in general  
608 circulation models, NASA Technical Memorandum No. 104606, Vol. 3, pp.85,1994.

609 Christensen, J.H., Christensen, O.B., Lopez, P., van Meijgaard, E. and Botzet, M.: The HIRHAM4  
610 regional atmospheric climate model. DMI Scientific report, 4, p.51, 1996.

611 Danielson, J.J. and Gesch, D.B.: Global multi-resolution terrain elevation data 2010 (GMTED2010) (No.  
612 2011-1073), US Geological Survey, 2011.

613 De Meij, A. and Vinuesa, J. F.: Impact of SRTM and Corine Land Cover data on meteorological  
614 parameters using WRF, *Atmos. Res.*, 143, 351–370, doi:10.1016/j.atmosres.2014.03.004, 2014.

615 Dee, D.P., Uppala, S.M., Simmons, A.J., Berrisford, P., Poli, P., Kobayashi, S., Andrae, U., Balmaseda,  
616 M.A., Balsamo, G., Bauer, D.P. and Bechtold, P.: The ERA-Interim reanalysis: Configuration and  
617 performance of the data assimilation system. *Quarterly Journal of the royal meteorological society*, 137,  
618 pp.553-597, <https://doi.org/10.1002/qj.828>, 2011.

619 Deep, A., Pandey, C.P., Nandan, H. et al. Evaluation of ambient air quality in Dehradun city during 2011–  
620 2014. *J Earth Syst Sci* 128, 96, doi:10.1007/s12040-019-1092-y, 2019.

621 Dimri, A.P., Chevuturi, A., Niyogi, D., Thayyen, R.J., Ray, K., Tripathi, S.N., Pandey, A.K. and Mohanty,  
622 U.C.: Cloudbursts in Indian Himalayas: a review. *Earth-science reviews*, 168, pp.1-23,  
623 <https://doi.org/10.1016/j.earscirev.2017.03.006>, 2017.

624 Ek, M.B., Mitchell, K.E., Lin, Y., Rogers, E., Grunmann, P., Koren, V., Gayno, G. and Tarpley, J.D.:  
625 Implementation of Noah land surface model advances in the National Centers for Environmental  
626 Prediction operational mesoscale Eta model. *Journal of Geophysical Research: Atmospheres*,  
627 <https://doi.org/10.1029/2002JD003296>, 2003.

628 Emery, C., Tai, E., and Yarwood, G.: Enhanced meteorological modeling and performance evaluation for two Texas  
629 ozone episodes, *Tech. Rep. Prepared for The Texas Natural Resource Conservation Commission, ENVIRON*  
630 *International Corporation*, 2001.

631 Farr, T.G., Rosen, P.A., Caro, E., Crippen, R., Duren, R., Hensley, S., Kobrick, M., Paller, M., Rodriguez,  
632 E., Roth, L. and Seal, D.: The shuttle radar topography mission, *Reviews of geophysics*, 45(2).  
633 doi:10.1029/2005RG000183, 2007.

634 Foley, A.M.: Uncertainty in regional climate modelling: A review. *Progress in Physical Geography*, 34,  
635 pp.647-670.<https://doi.org/10.1177/0309133310375654>, 2010.

636 Gao, Y., Xu, J. and Chen, D.: Evaluation of WRF mesoscale climate simulations over the Tibetan Plateau during  
637 1979-2011, *J. Clim.*, 28(7), 2823–2841, doi:10.1175/JCLI-D-14-00300.1, 2015.

638 Hanna, S. R. and Yang, R.: Evaluations of Mesoscale Models' Simulations of Near-Surface Winds, Temperature  
639 Gradients, and Mixing Depths, *J. Appl. Meteorol.*, 40(6), 1095–1104, doi:10.1175/1520-  
640 0450(2001)040<1095:EOMMSO>2.0.CO;2, 2001.

641 Hart, K. A., Steenburgh, W. J. and Onton, D. J.: Model Forecast Improvements with Decreased Horizontal Grid  
642 Spacing over Finescale Intermountain Orography during the 2002 Olympic Winter Games, *Weather Forecast.*,  
643 20(4), 558–576, doi:10.1175/WAF865.1, 2005.

644 Hong, S.Y., Noh, Y. and Dudhia, J.: A new vertical diffusion package with an explicit treatment of  
645 entrainment processes. *Monthly weather review*, 134, pp.2318-2341,  
646 <https://doi.org/10.1175/MWR3199.1>, 2006.

647 Kain, J.S.: The Kain–Fritsch convective parameterization: an update. *Journal of applied meteorology*, 43,  
648 pp.170-181, [https://doi.org/10.1175/1520-0450\(2004\)043<0170:TKCPAU>2.0.CO;2](https://doi.org/10.1175/1520-0450(2004)043<0170:TKCPAU>2.0.CO;2), 2004.

649 Kotamarthi, V.R.: Ganges Valley Aerosol Experiment (GVAX) Final Campaign Report. DOE/SC-ARM-  
650 14-011, available at: <https://www.arm.gov/publications/programdocs/doe-sc-arm-14-011>. Pdf, 2013.

651 Kumar, R., Naja, M., Pfister, G.G., Barth, M.C. and Brasseur, G.P.: Simulations over South Asia using  
652 the Weather Research and Forecasting model with Chemistry (WRF-Chem): set-up and meteorological  
653 evaluation. *Geoscientific Model Development*, 5, p.321, <https://doi.org/10.5194/gmd-5-321-2012>, 2012.

654 Laprise, R. Regional climate modelling. *Journal of Computational Physics*, 227, pp.3641-3666.,  
655 <https://doi.org/10.1016/j.jcp.2006.10.024>, 2008.

656 Lawrence, M.G. and Lelieveld, J.: Atmospheric pollutant outflow from southern Asia: a review.  
657 *Atmospheric Chemistry and Physics*, 10, p.11017, <https://doi.org/10.5194/acp-10-11017-2010>, 2010.

658 Lee, T. J., Pielke, R. A., Kessler, R. C. and Weaver, J.: Influence of Cold Pools Downstream of Mountain Barriers  
659 on Downslope Winds and Flushing, *Mon. Weather Rev.*, 117(9), 2041–2058, doi:10.1175/1520-  
660 0493(1989)117<2041:IOCPDO>2.0.CO;2, 1989.

661 Lelieveld, J., Bourtsoukidis, E., Brühl, C., Fischer, H., Fuchs, H., Harder, H., Hofzumahaus, A., Holland,  
662 F., Marno, D., Neumaier, M. and Pozzer, A.: The South Asian monsoon—pollution pump and purifier.  
663 Science, 361, pp.270-273, DOI:10.1126/science.aar2501, 2018.

664 Mar, K. A., Ojha, N., Pozzer, A. and Butler, T. M.: Ozone air quality simulations with WRF-Chem (v3.5.1) over  
665 Europe: Model evaluation and chemical mechanism comparison, *Geosci. Model Dev.*, 9(10), 3699–3728,  
666 doi:10.5194/gmd-9-3699-2016, 2016.

667 Mass, C. F., Ovens, D., Westrick, K. and Colle, B. A.: DOES INCREASING HORIZONTAL RESOLUTION  
668 PRODUCE MORE SKILLFUL FORECASTS?: The Results of Two Years of Real-Time Numerical Weather  
669 Prediction over the Pacific Northwest, *Bull. Am. Meteorol. Soc.*, 83(3), 407–430, doi:10.1175/1520-  
670 0477(2002)083<0407:DIHRPM>2.3.CO;2, 2002.

671 Meher, J.K., Das, L., Akhter, J., Benestad, R.E. and Mezghani, A.: 2017. Performance of CMIP3 and  
672 CMIP5 GCMs to simulate observed rainfall characteristics over the Western Himalayan region. *Journal of*  
673 *Climate*, 30, pp.7777-7799, <https://doi.org/10.1175/JCLI-D-16-0774.1>, 2017.

674 Mlawer, E.J., Taubman, S.J., Brown, P.D., Iacono, M.J. and Clough, S.A.: Radiative transfer for  
675 inhomogeneous atmospheres: RRTM, a validated correlated-k model for the longwave. *Journal of*  
676 *Geophysical Research: Atmospheres*, 102, pp.16663-16682. <https://doi.org/10.1029/97JD00237>, 1997.

677 Mues, A., Lauer, A., Lupascu, A., Rupakheti, M., Kuik, F. and Lawrence, M.G.: WRF and WRF-Chem  
678 v3. 5.1 simulations of meteorology and black carbon concentrations in the Kathmandu Valley.  
679 *Geoscientific Model Development*, 11, p.2067. <https://doi.org/10.5194/gmd-11-2067-2018>, 2018.

680 Naja, M., Bhardwaj, P., Singh, N., Kumar, P., Kumar, R., Ojha, N., Sagar, R., Satheesh, S. K., Krishna  
681 Moorthy, K., Kotamarthi, V. R., High-frequency vertical profiling of meteorological parameters using  
682 AMF1 facility during RAWEX–GVAX at ARIES, Nainital, *Current Science*, Vol. 111, No. 1, 132–140,  
683 2016.

684 Nandargi, S. and Dhar, O.N.: Extreme rainstorm events over the northwest Himalayas during 1875–2010.  
685 *Journal of Hydrometeorology*, <https://doi.org/10.1175/JHM-D-12-08.1>, 2012.

686 Ojha, N., Girach, I., Sharma, K., Nair, P., Singh, J., Sharma, N., Singh, N., Flemming, J., Inness, A. and  
687 Subrahmanyam, K.V.: Surface ozone in the Doon Valley of the Himalayan foothills during spring.  
688 *Environ. Sci. Poll. Res.*, doi:10.1007/s11356-019-05085-2, 2019

689 Ojha, N., Naja, M., Singh, K.P., Sarangi, T., Kumar, R., Lal, S., Lawrence, M.G., Butler, T.M. and  
690 Chandola, H.C.: Variabilities in ozone at a semi-urban site in the Indo-Gangetic Plain region: Association

691 with the meteorology and regional processes. *Journal of Geophysical Research: Atmospheres*,  
692 <https://doi.org/10.1029/2012JD017716>, 2012.

693 Ojha, N., Pozzer, A., Rauthe-Schöch, A., Baker, A.K., Yoon, J., Brenninkmeijer, C.A. and Lelieveld, J.:  
694 Ozone and carbon monoxide over India during the summer monsoon: regional emissions and transport.  
695 *Atmos. Chem. Phys.*, <https://doi.org/10.5194/acp-16-3013-2016>, 2016.

696 Pant, G.B., Pradeep Kumar, P., V. Revadekar, Jayashree, Singh, Narendra.: *The Himalaya*.  
697 <https://doi.org/10.1007/978-3-319-61654-4>, 2018.

698 Pant, P., Hegde, P., Dumka, U.C., Sagar, R., Satheesh, S.K., Moorthy, K.K., Saha, A. and Srivastava,  
699 M.K.: Aerosol characteristics at a high-altitude location in central Himalayas: Optical properties and  
700 radiative forcing. *Journal of Geophysical Research: Atmospheres*. <https://doi.org/10.1029/2005JD006768>,  
701 2006.

702 Pervez, M.S. and Henebry, G.M.: Projections of the Ganges–Brahmaputra precipitation—Downscaled  
703 from GCM predictors. *Journal of Hydrology*, 517, pp.120-  
704 134.<https://doi.org/10.1016/j.jhydrol.2014.05.016>, 2014.

705 Rife, D. L. and Davis, C. A.: *Verification of Temporal Variations in Mesoscale Numerical Wind Forecasts*, *Mon.*  
706 *Weather Rev.*, 133(11), 3368–3381, [doi:10.1175/MWR3052.1](https://doi.org/10.1175/MWR3052.1), 2005.

707 Rupakheti, D., Adhikary, B., Praveen, P.S., Rupakheti, M., Kang, S., Mahata, K.S., Naja, M., Zhang, Q.,  
708 Panday, A.K. and Lawrence, M.G., 2017.: Pre-monsoon air quality over Lumbini, a world heritage site  
709 along the Himalayan foothills. *Atmos. Chem. Phys.*, 17, 11041-11063, [https://doi.org/10.5194/acp-17-](https://doi.org/10.5194/acp-17-11041-2017)  
710 11041-2017, 2017.

711 Sarangi, T., Naja, M., Ojha, N., Kumar, R., Lal, S., Venkataramani, S., Kumar, A., Sagar, R. and Chandola,  
712 H.C.: First simultaneous measurements of ozone, CO, and NO<sub>y</sub> at a high-altitude regional representative  
713 site in the central Himalayas. *Journal of Geophysical Research: Atmospheres*, 119, pp.1592-1611.  
714 <https://doi.org/10.1002/2013JD020631>, 2014.

715 Sharma, A., Ojha, N., Pozzer, A., Mar, K. A., Beig, G., Lelieveld, J., and Gunthe, S. S.: WRF-Chem  
716 simulated surface ozone over south Asia during the pre-monsoon: effects of emission inventories and  
717 chemical mechanisms, *Atmos. Chem. Phys.*, 17, 14393–14413, [https://doi.org/10.5194/acp-17-14393-](https://doi.org/10.5194/acp-17-14393-2017)  
718 2017, 2017.

719 Sharma, S.S. and Ganju, A.: Complexities of avalanche forecasting in Western Himalaya—an  
720 overview. *Cold Regions Science and Technology*, 31, pp.95-102. <https://doi.org/10.1016/S0165->  
721 232X(99)00034-8\_2000.

722 Singh, N., Solanki, R., Ojha, N., Janssen, R.H., Pozzer, A. and Dhaka, S.K.: Boundary layer evolution  
723 over the central Himalayas from radio wind profiler and model simulations. *Atmospheric Chemistry &*  
724 *Physics*, <https://doi.org/10.5194/acp-16-10559-2016>, 2016.

725 Skamarock, W. C., Klemp, J.B., Dudhia, J., Gill, D.O., Barker, D.M., Wang, W. and Powers, J.G.: A  
726 Description of the Advanced Research WRF Version 3. NCAR Technical Note NCAR/TN-475+STR,  
727 <http://dx.doi.org/10.5065/D68S4MVH>, 2008.

728 Solanki, R., Singh, N., Kumar, N.K., Rajeev, K. and Dhaka, S.K.: Time variability of surface-layer  
729 characteristics over a mountain ridge in the central Himalayas during the spring season. *Boundary-layer*  
730 *meteorology*, 158, pp.453-471, <https://doi.org/10.1007/s10546-015-0098-5>, 2016.

731 Solanki, R., Singh, N., Kiran Kumar, N. V. P., Rajeev, K., Imasu, R. and Dhaka, S. K.: Impact of  
732 Mountainous Topography on Surface-Layer Parameters During Weak Mean-Flow Conditions, *Boundary-*  
733 *Layer Meteorol.*, 172(1), 133–148, doi:10.1007/s10546-019-00438-3, 2019.

734 Srivastava, A.K., Ram, K., Pant, P., Hegde, P. and Joshi, H.: Black carbon aerosols over Manora Peak in  
735 the Indian Himalayan foothills: implications for climate forcing. *Environmental Research Letters*, 7,  
736 p.014002, 2012.

737 Sun, X.B., Ren, G.Y., Shrestha, A.B., Ren, Y.Y., You, Q.L., Zhan, Y.J., Xu, Y. and Rajbhandari, R.:  
738 Changes in extreme temperature events over the Hindu Kush Himalaya during 1961–2015. *Advances in*  
739 *Climate Change Research*, <https://doi.org/10.1016/j.accre.2017.07.001>, 2017.

740 Taylor, K.E.: Summarizing multiple aspects of model performance in a single diagram. *Journal of*  
741 *Geophysical Research: Atmospheres*, 106, pp.7183-7192, <https://doi.org/10.1029/2000JD900719>, 2001.

742 Teixeira, J. C., Carvalho, A. C., Carvalho, M. J., Luna, T. and Rocha, A.: Sensitivity of the WRF model  
743 to the lower boundary in an extreme precipitation event-Madeira island case study, *Nat. Hazards Earth*  
744 *Syst. Sci.*, 14(8), 2009–2025, doi:10.5194/nhess-14-2009-2014, 2014.

745 Tewari, M., Chen, F., Wang, W., Dudhia, J., LeMone, M.A., Mitchell, K., Ek, M., Gayno, G., Wegiel, J.  
746 and Cuenca, R.H.: Implementation and verification of the unified NOAA land surface model in the WRF  
747 model. In 20th conference on weather analysis and forecasting/16th conference on numerical weather  
748 prediction (Vol. 1115) , 2004,

749 Thompson, G., Rasmussen, R.M. and Manning, K.: Explicit forecasts of winter precipitation using an  
750 improved bulk microphysics scheme. Part I: Description and sensitivity analysis. *Monthly Weather*  
751 *Review*, 132(2), pp.519-542, [https://doi.org/10.1175/1520-0493\(2004\)132<0519:EFOWPU>2.0.CO;2](https://doi.org/10.1175/1520-0493(2004)132<0519:EFOWPU>2.0.CO;2),  
752 2004.

753 Tiwari, P.R., Kar, S.C., Mohanty, U.C., Dey, S., Sinha, P. and Shekhar, M.S.: Sensitivity of the Himalayan  
754 orography representation in simulation of winter precipitation using Regional Climate Model (RegCM)  
755 nested in a GCM. *Climate Dynamics*, 49(11-12), pp.4157-4170, [https://doi.org/10.1007/s00382-017-](https://doi.org/10.1007/s00382-017-3567-3)  
756 3567-3, 2017.

757 Tselioudis, G., Douvis, C. and Zerefos, C.: Does dynamical downscaling introduce novel information in  
758 climate model simulations of precipitation change over a complex topography region? *International*  
759 *Journal of Climatology*, 32, pp.1572-1578, <https://doi.org/10.1002/joc.2360>, 2012.

760 Vincent, C. L. and Hahmann, A. N.: The impact of grid and spectral nudging on the variance of the near-  
761 surface wind speed, *J. Appl. Meteorol. Climatol.*, 54(5), 1021–1038, doi:10.1175/JAMC-D-14-0047.1,  
762 2015.

763 Wang, Y., Leung, L.R., McGREGOR, J.L., Lee, D.K., Wang, W.C., Ding, Y. and Kimura, F.: Regional  
764 climate modeling: progress, challenges, and prospects. *Journal of the Meteorological Society of Japan*.  
765 Ser. II, 82, pp.1599-1628, <https://doi.org/10.2151/jmsj.82.1599>, 2004.

766 Wang, Y., Yang, K., Zhou, X., Chen, D., Lu, H., Ouyang, L., Chen, Y., Lazhu and Wang, B.: Synergy of  
767 orographic drag parameterization and high resolution greatly reduces biases of WRF-simulated precipitation in  
768 central Himalaya, *Clim. Dyn.*, 54(3), 1729–1740, doi:10.1007/s00382-019-05080-w, 2020.

769 Weisman, M.L., Skamarock, W.C. and Klemp, J.B.: The resolution dependence of explicitly modeled  
770 convective systems. *Monthly Weather Review*, 125, pp.527-548, [https://doi.org/10.1175/1520-](https://doi.org/10.1175/1520-0493(1997)125<0527:TRDOEM>2.0.CO;2)  
771 0493(1997)125<0527:TRDOEM>2.0.CO;2, 1997.

772 Wilby, R.L., Hay, L.E. and Leavesley, G.H.: A comparison of downscaled and raw GCM output:  
773 implications for climate change scenarios in the San Juan River basin, Colorado. *Journal of Hydrology*,  
774 225, pp.67-91, [https://doi.org/10.1016/S0022-1694\(99\)00136-5](https://doi.org/10.1016/S0022-1694(99)00136-5), 1999.

775 Xue, Y., Janjic, Z., Dudhia, J., Vasic, R. and De Sales, F.: A review on regional dynamical downscaling  
776 in intraseasonal to seasonal simulation/prediction and major factors that affect downscaling ability, *Atmos.*  
777 *Res.*, 147–148, 68–85, doi:10.1016/j.atmosres.2014.05.001, 2014.

778 Yver, C. E., Graven, H. D., Lucas, D. D., Cameron-Smith, P. J., Keeling, R. F. and Weiss, R. F.: Evaluating  
779 transport in the WRF model along the California coast, *Atmos. Chem. Phys.*, 13(4), 1837–1852, doi:10.5194/acp-  
780 13-1837-2013, 2013.

781 Zadra, A., Caya, D., Côté, J.E.A.N., Dugas, B., Jones, C., Laprise, R., Winger, K. and Caron, L.P.: The  
782 next Canadian regional climate model. *PhysCan*, 64, pp.75-83, 2008.

783 Zhang, D. L. and Zheng, W. Z.: Diurnal cycles of surface winds and temperatures as simulated by five boundary  
784 layer parameterizations, *J. Appl. Meteorol.*, 43(1), 157–169, doi:10.1175/1520-  
785 0450(2004)043<0157:DCOSWA>2.0.CO;2, 2004.

786 Zhang, Y., Sartelet, K., Wu, S. Y. and Seigneur, C.: Application of WRF/Chem-MADRID and WRF/Polyphemus  
787 in Europe - Part 1: Model description, evaluation of meteorological predictions, and aerosol-meteorology  
788 interactions, *Atmos. Chem. Phys.*, 13(14), 6807–6843, doi:10.5194/acp-13-6807-2013, 2013.

789 Zhou, X., Beljaars, A., Wang, Y., Huang, B., Lin, C., Chen, Y. and Wu, H.: Evaluation of WRF Simulations With  
790 Different Selections of Subgrid Orographic Drag Over the Tibetan Plateau, *J. Geophys. Res. Atmos.*, 122(18),  
791 9759–9772, doi:10.1002/2017JD027212, 2017.

792 Zhou, X., Yang, K. and Wang, Y.: Implementation of a turbulent orographic form drag scheme in WRF and its  
793 application to the Tibetan Plateau, *Clim. Dyn.*, 50(7–8), 2443–2455, doi:10.1007/s00382-017-3677-y, 2018.

794 Zhou, X., Yang, K., Beljaars, A., Li, H., Lin, C., Huang, B. and Wang, Y.: Dynamical impact of parameterized  
795 turbulent orographic form drag on the simulation of winter precipitation over the western Tibetan Plateau, *Clim.*  
796 *Dyn.*, 53(1–2), 707–720, doi:10.1007/s00382-019-04628-0, 2019.

*Supplementary material*

## **Effects of spatial resolution on WRF v3.8.1 simulated meteorology over the central Himalaya**

**Jaydeep Singh<sup>1</sup>, Narendra Singh<sup>1\*</sup>, Narendra Ojha<sup>2</sup>, Amit Sharma<sup>3, a</sup>, Andrea Pozzer<sup>4, 5\*</sup>, Nadimpally Kiran Kumar<sup>6</sup>, Kunjukrishnapillai Rajeev<sup>6</sup>, Sachin S. Gunthe<sup>3</sup>, V. Rao Kotamarthi<sup>7</sup>**

<sup>1</sup>Aryabhata Research Institute of Observational Sciences, Nainital, India

<sup>2</sup>Physical Research Laboratory, Ahmedabad, India

<sup>3</sup>EWRE Division, Department of Civil Engineering, Indian Institute of Technology Madras, Chennai, India

<sup>4</sup>Department of Atmospheric Chemistry, Max Planck Institute for Chemistry, Mainz, Germany

<sup>5</sup>Earth System Physics Section, International Centre for Theoretical Physics, Trieste, Italy

<sup>6</sup>Space Physics Laboratory, Vikram Sarabhai Space Centre, Thiruvananthapuram, India

<sup>7</sup>Environmental Science Division, Argonne National Laboratory, Argonne, Illinois, USA

<sup>a</sup>Now at Department of Civil and Infrastructural Engineering, Indian Institute of Technology Jodhpur, Jodhpur, India

**Correspondence:** Narendra Singh (narendra@aries.res.in) and Andrea Pozzer (andrea.pozzer@mpic.de)

**Evaluation metrics:** The following statistical metrics are used to evaluate the WRF model performance.

**Mean Bias (MB)**

$$\text{MB} = \frac{1}{N} \sum_{i=1}^N (P_i - O_i)$$

**RMSE (Root mean square error)**

$$\text{RMSE} = \sqrt{\frac{\sum_{i=1}^N (P_i - O_i)^2}{N}}$$

**Correlation coefficient (r)**

$$r = \frac{1}{N-1} \sum_{i=1}^N \frac{(P_i - \bar{P})(O_i - \bar{O})}{\sigma_P \sigma_O}$$

Where:

$N$  = The total number of the total pairs of observations and model simulated values

$P$  = The model values

$O$  = The observations

$\sigma_P$  and  $\sigma_O$  are the standard deviation of the and observations.

**Table S1.** The summary of the statistical metrics MB, RMSE and correlation coefficient (r) for different meteorological parameters, surface pressure (P), 2m temperature (T2), 2m relative humidity (RH2), 10m wind speed (WS10) and specific humidity (Q2) within all three domains d01, d02 and d03 without the altitude adjustment and after altitude correction

Parameters	MB						RMSE						Correlation Coefficient (r)					
	Without correction			With correction			Without correction			With correction			Without correction			With correction		
	d01	d02	d03	d01	d02	d03	d01	d02	d03	d01	d02	d03	d01	d02	d03	d01	d02	d03
P (hPa)	65.3	32.5	25.2	0.1	0.1	0.1	66.8	33.3	25.8	0.6	0.6	0.6	0.97	0.97	0.97	0.97	0.97	0.97
T2 (°C)	2.8	0.9	0.2	-1.1	-1.2	-1.2	3.2	1.6	1.3	1.9	2.0	2.0	0.75	0.67	0.67	0.35	0.34	0.36
RH2 (%)	-6.4	-0.4	-2.4	-8.4	-0.9	-3.1	12.1	8.8	8.9	12.8	10.0	10.4	0.43	0.45	0.52	0.56	0.39	0.46
WS10 (ms <sup>-1</sup> )	0.0	0.9	0.5	1.3	2.7	1.9	1.6	2.0	2.0	2.8	4.0	3.5	0.18	0.18	0.24	0.35	0.33	0.34
Q2 (g Kg <sup>-1</sup> )	0.4	0.3	-0.7	-2.4	-1.3	-1.6	1.6	1.5	1.6	3.0	1.9	2.2	0.67	0.72	0.77	0.63	0.68	0.72

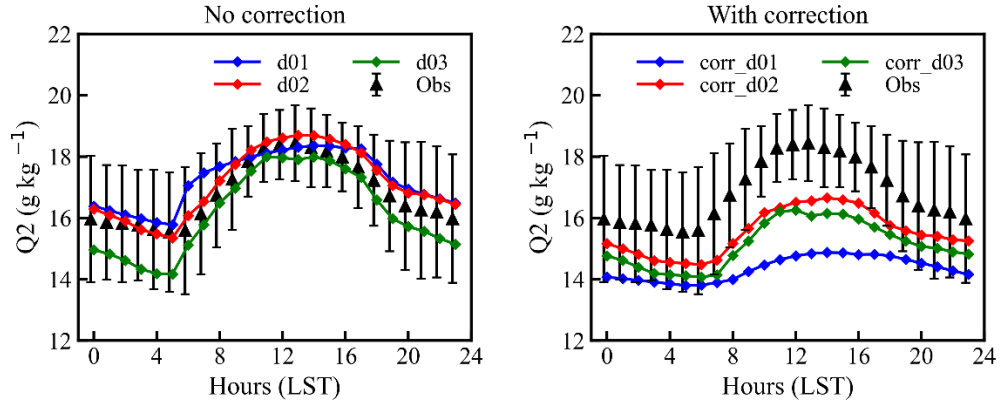


**Fig. S1** The diurnal variation of the 2m specific humidity (Q2) in different domain. The left panel for without altitude adjustment and right panel after the correction of the altitude.

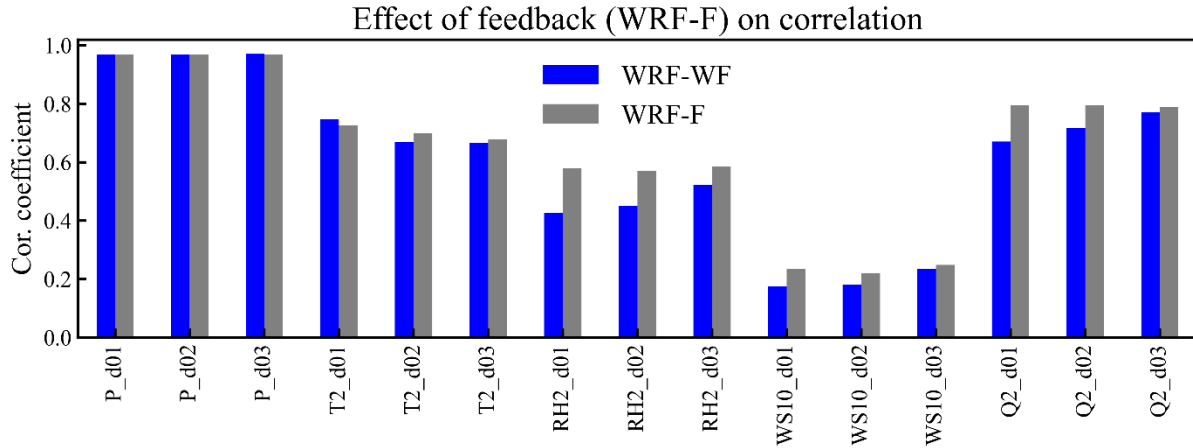


**Fig. S2** The comparison of the correlation coefficients without feedback (WRF-WF: blue) and with feedback (WRF-F: gray) for different meteorological parameters; Surface pressure (P), 2m temperature (T2), 2m relative humidity (RH2), 10m wind speed (WS10) and 2m Specific Humidity (Q2) for the different domains d01, d02 and d03

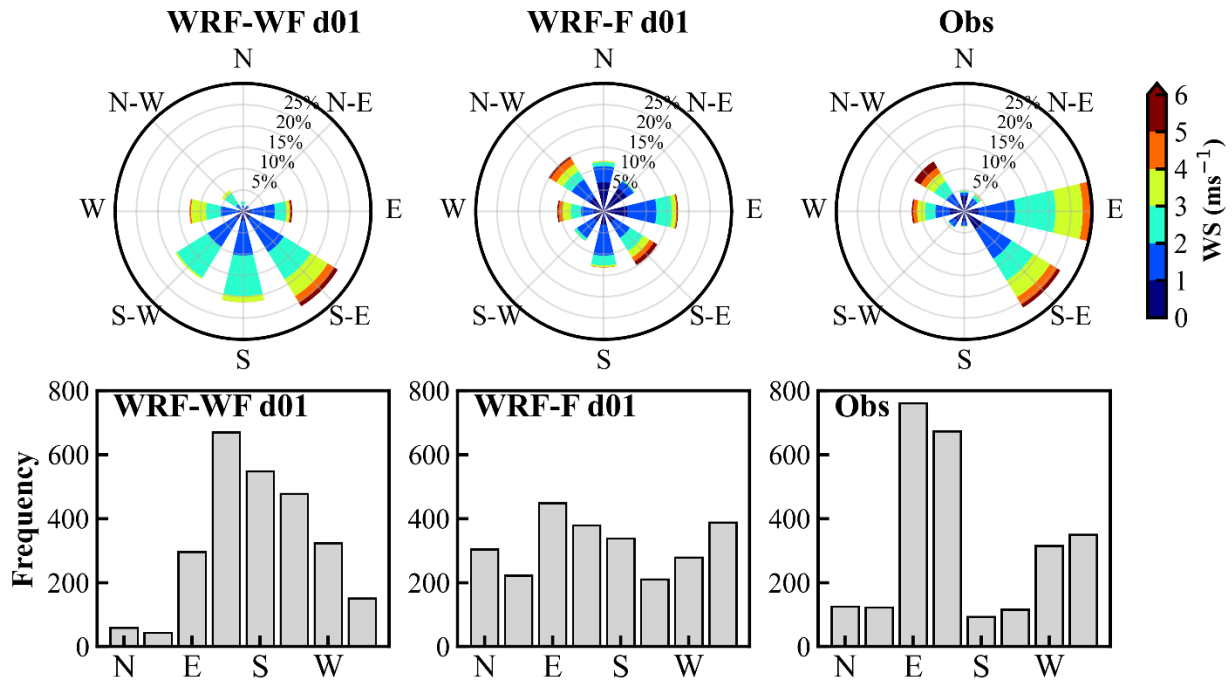


**Fig S3:** Comparison of the wind speed and direction is shown by the windrose diagram (first row), and frequency distribution of the wind direction (second row) for d01 without feedback

(WRF-WF) and with feedback (WRF-F) along with the observation for the time period June-September 2011. The different colours of windrose show the wind speed and the radius of windrose show the percentage frequency of counts for particular direction.

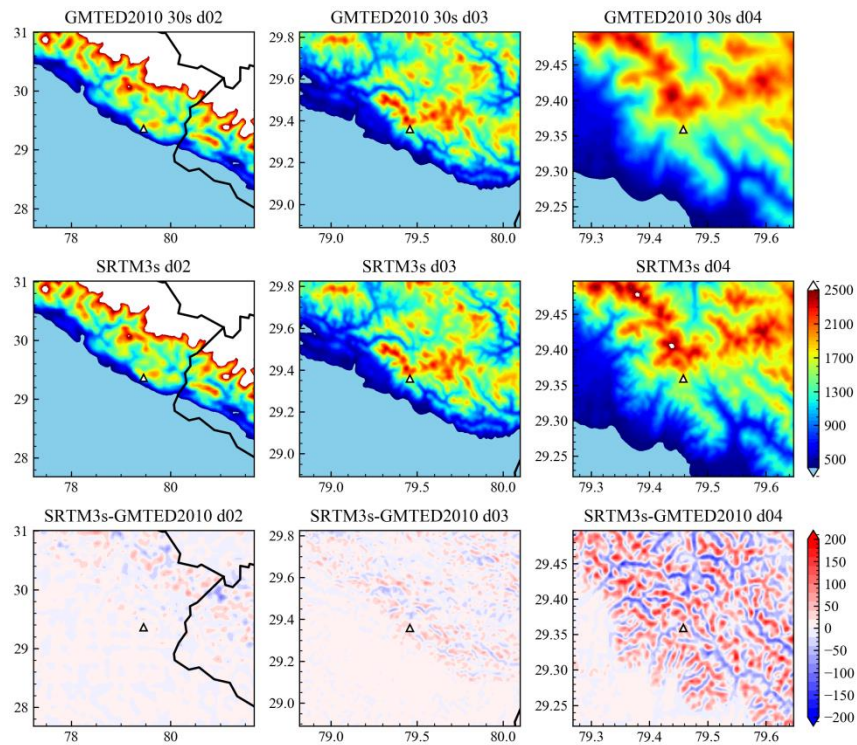


**Figure S4:** The topography from GMTED2010 (first row) at 30s and SRTM (second row) at 3s in three different domain d02, d03 and d04 while third row shows the difference between SRTM and GMTED2010.

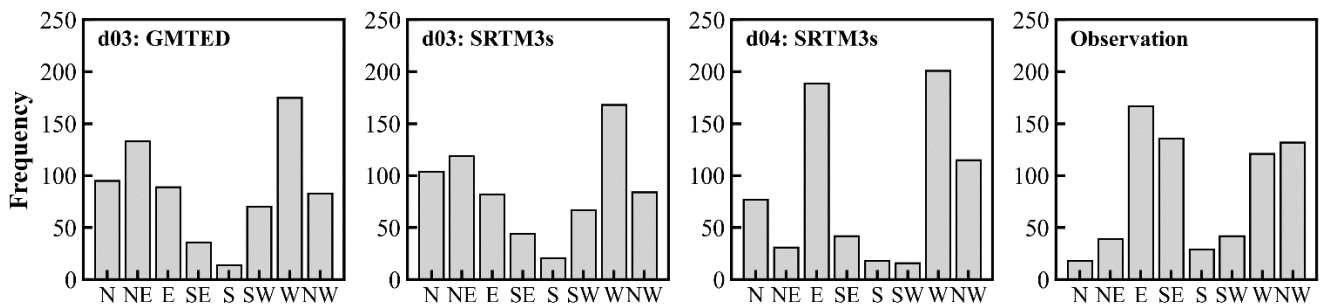


**Figure S5:** Frequency distribution of wind direction

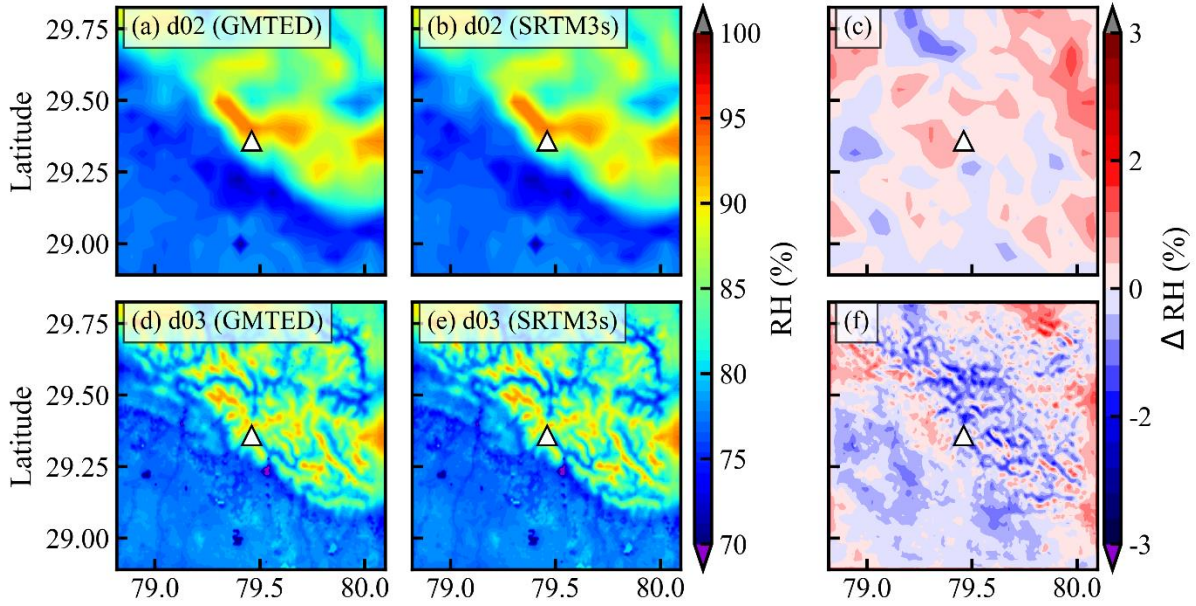


**Figure S6:** Mean distribution of relative humidity (RH; %) during 1–30 September 2011 simulated by WRF model (a) d02 from GMTED, and (b) d02 using SRTM3s; (c) the difference between (a) and (b) while in d03 is shown from (d-f). The triangle shows the observation station.